Electronic Supplementary Information

for

Metal-Free, Regioselective and Stereoregular Alternating Copolymerization of Monosubstituted Epoxides and Tricyclic Anhydrides

He-Yuan Ji,[a] Xiao-Lu Chen,[a] Bin Wang,*[,a] Li Pan,[a] Yue-Sheng Li *[,a,b]

[a]Tianjin Key Lab of Composite & Functional Materials, School of Materials Science and Engineering, Tianjin University, Tianjin 300350, China

[b]Collaborative Innovation Center of Chemical Science and Engineering (Tianjin), Tianjin 300072, China.

Table of Contents

1. Experimental Procedures

Reagents. Unless otherwise stated, all chemicals are used without further purification. BEt_3, propylene oxide (PO), 1,2-Hexene oxide (HO), styrene oxide (SO), *S*-SO, allyl glycidyl ether (AGE) and furfuryl glycidyl ether (FGE) were purchased from Acros. *Endo*-3a,4,7,7a-Tetrahydro-4,7-Methanoisobenzofuran-1,3-dione (*endo*-CPMA), bis(triphenylphosphine)iminium chloride (PPNCl), 4-dimethylaminopyridine (DMAP) and P^nBu_3 were purchased from Energy Chemical. *Exo*-7-Oxabicyclo[2.2.1]hept-5-ene-2,3-dicarboxylic anhydride, phenyl glycidyl ether (PGE), $B(C_6F_5)_3$ and $B(C_6H_5)_3$ were purchased from Alfa Aesar. Tert-Butylimino-tris(dimethylamino)phosphorane (P_1-*t*-Bu) was purchased from Aldrich. *Exo*-3a,4,7,7a-Tetrahydro-4,7-Methanoisobenzofuran-1,3-dione (*exo*-CPMA), *endo*-3a,4,7,7a-Tetrahydro-4,7-ethanoisobenzofuran-1,3-dione (*endo*-CHMA), benzyl glycidyl ether (BGE) and *S*-BGE were purchased from Ark Pharm. 1,3-Bis(2,4,6-trimethylphenyl) imidazol-2-ylidene (IMes) was purchased from Strem. *S*-PO was purchased from Innochem. 1,2-Butylene Oxide (BO), *S*-BO, *S*-HO and *S*-PGE were purchased from TCI. *Endo*-CPMA, *endo*-CHMA, and *exo*-CPMA were purified three times by the way of sublimation. *Exo*-FMA was used as received. PO, BO, HO, SO, AGE, BGE, FGE, PGE, *S*-PO, *S*-BO, *S*-HO, *S*-SO, *S*-BGE and *S*-PGE were dried over CaH_2 for 48 h, distilled, and stored under nitrogen atmosphere. DMAP was recrystallized from anhydrous ethyl acetate before use. All manipulations were performed using a standard Schlenk technique or in a nitrogen-filled Etelux Lab2000 glovebox unless otherwise mentioned.

General copolymerization procedure. In an Etelux glovebox, the appropriate amount of Lewis acid (0.02 mmol, 1 equiv.), Lewis base (0.02 mmol) and cyclic anhydride (2 mmol, 100 equiv.) were added in an oven-dried tube equipped with a magnetic stir bar, followed by epoxide (10 mmol, 500 equiv.). The tube was sealed with a Teflon cap. Subsequently, the tube was removed from the glovebox and placed in an aluminum heating block with predetermined temperature. After the defined time, a crude aliquot was withdrawn from the system by pipette and monitored by ^1H NMR spectroscopy in $CDCl_3$ to determine monomer conversion. The reaction mixture was diluted with approximately 10 mL dichloromethane and precipitated into 100 mL of methanol acidified by hydrochloric acid with vigorous stirring, after which the methanol was filtrated or decanted. The resulting polymers were dried under vacuum at 40 °C. All analyses were performed on the crude samples.

Determination of regioselective ring-opening of terminal epoxides. A round-bottomed flask was charged with polyesters obtained from enantiopure terminal epoxides (*S*-PO and *S*-BO) (100 mg), THF (10 mL), MeOH (2 mL) and NaOH (4 mol/L, 2 mL). The resultant mixture was stirred at room temperature for 24 h. Then, it was concentrated to about 8 mL by evaporation. The solution was extracted

with ethyl acetate (10 mL × 3). The combined organic layers were dried over anhydrous $MgSO_4$; and then the mixture was filtered and evaporated to colorless or yellow oil with a spot of ethyl acetate. The enantiomeric excess (*ee*) of the resultant diols was determined by Agilent 7890A gas chromatography (GC) analysis equipped with a hydrogen flame ionization detector (FID) and a chiral GC column (Agilent CycloSil-B 30 m × 0.25 mm ID × 0.25 μm film). Retention time of diols and separation methods were showed as follows:

1,2-Propanediol: Injection temperature 275 ºC; FID detection temperature 275 ºC; Oven temperature 60 ºC. Retention time of *S*-1,2-propanediol = 28.6 min; Retention time of *R*-1,2-propanediol = 29.7 min.

1,2-Butanediol: Injection temperature 275 ºC; FID detection temperature 275 ºC; Oven temperature 70 ºC. Retention time of *S*-1,2-Butanediol = 23.5 min; Retention time of *R*-1,2-Butanediol = 27.1 min.

Styrene glycol: Injection temperature 275 ºC; FID detection temperature 275 ºC; Oven temperature 140 ºC. Retention time of *R*-styrene glycol = 29.6 min; Retention time of *S*-styrene glycol = 30.6 min.

3-Benzyloxy-1,2-propanediol: Injection temperature 275 ºC; FID detection temperature 275 ºC; Oven temperature 220 ºC. Retention time of *R*-1,2-Hexanediol = 21.5 min; Retention time of *S*-1,2-Hexanediol = 26.4 min.

3-Phenoxy-1,2-propanediol: Injection temperature 275 ºC; FID detection temperature 275 ºC; Oven temperature 180 ºC. Retention time of *S*-1,2-Hexanediol = 24.3 min; Retention time of *R*-1,2-Hexanediol = 26.0 min.

Methods. ^{1}H, ^{13}C and 2D NMR spectra were recorded on a Bruker Avance III 400 MHz spectrometer at room temperature in chloroform-d_1, and chemical shifts were referenced to an internal standard (TMS). Gel permeation chromatography (GPC) analyses were carried out at 40 °C and a flow rate of 1.0 mL/min, with THF as the eluent on an Agilent PL-GPC 50 instrument coupled with a refractive index (RI) detector with respect to polystyrene (PS) standards. The columns included a PLgel guard 50 × 7.5 mm column, a PLgel mixed-B 300 × 7.5 mm column and a PLgel mixed-C 300 × 7.5 mm column. Samples being tested were filtered through a 0.22 μm PTFE filter. Chiral GC analyses were carried out at an Agilent 7890A instrument equipped with an FID and a chiral GC column (Agilent CycloSil-B 30 m × 0.25 mm ID × 0.25 μm film). Differential scanning calorimetry (DSC) analyses of polymer samples were carried out at a scanning speed of 10 ºC/min (from -20 ºC to 180 ºC) on a TA instruments DSC Q2000 with three heating cycles. Wide angle X-ray diffraction (WAXD) analyses of polymer powder were performed on an EMPYREAN diffractometer with Cu KR radiation (λ = 1.54056 Å) over the 2θ range of 5-80^{o} with a scan speed of 7.5^{o}/min at room temperature. The samples for WAXD are from the isolated polymers after precipitation from methanol and drying under vacuum.

2. The fate of the borane catalyst

Generally, BEt_3 would convert into Et_2BOMe and/or $EtB(OMe)_2$ upon mixing anhydrous methanol. Borane and the resultant boronic acid esters could convert into nontoxic boric acid in the presence of proton acids or moisture. Therefore, it is not necessary to purify the polymers by precipitation in acidified methanol. If the reaction mixture was precipitated in acidified methanol, nontoxic boric acid could be fully removed from polymers, evidenced by ^{11}B NMR spectra. In this work, we isolate polymers by precipitation since the process is simple to remove unreacted anhydrides and epoxides.

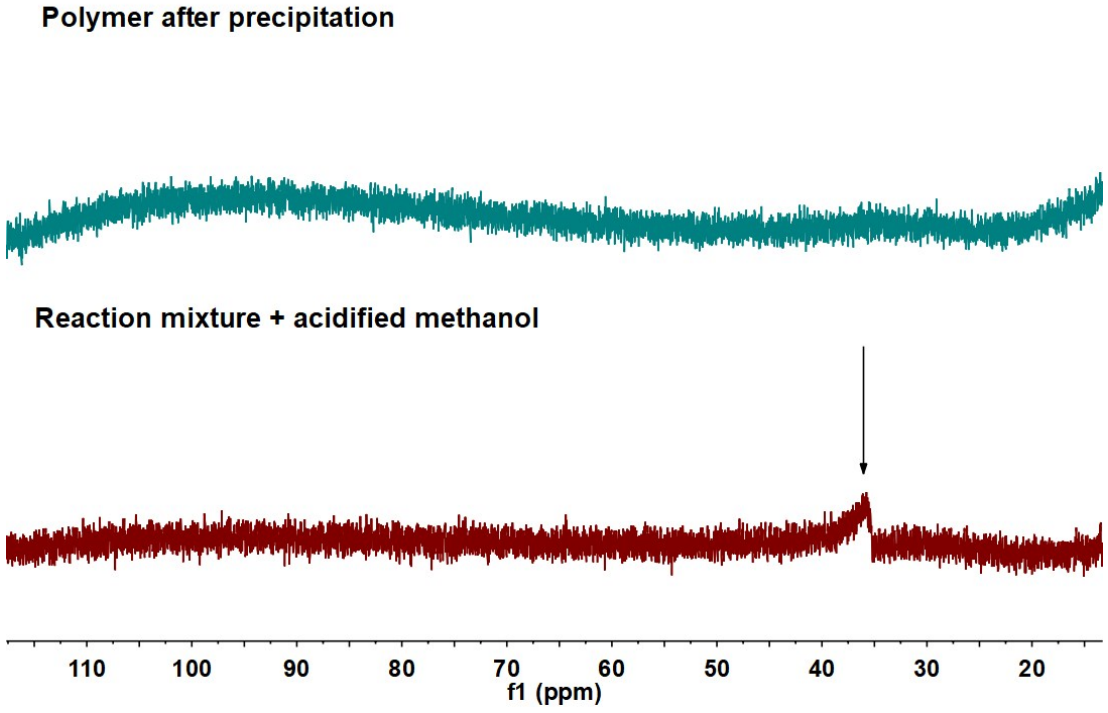

Figure S1. The ^{11}B NMR spectra of the reaction mixture and the resulting copolymer by precipitation in $CDCl_3$.

3. ^{1}H NMR spectrum of the resulting copolymers without chemoselectivity

The ROAC of *endo*-CPMA and PO catalyzed by $B(C_6F_5)_3$/PPNCl resulted in severe etherification with little *endo*-CPMA inserted.

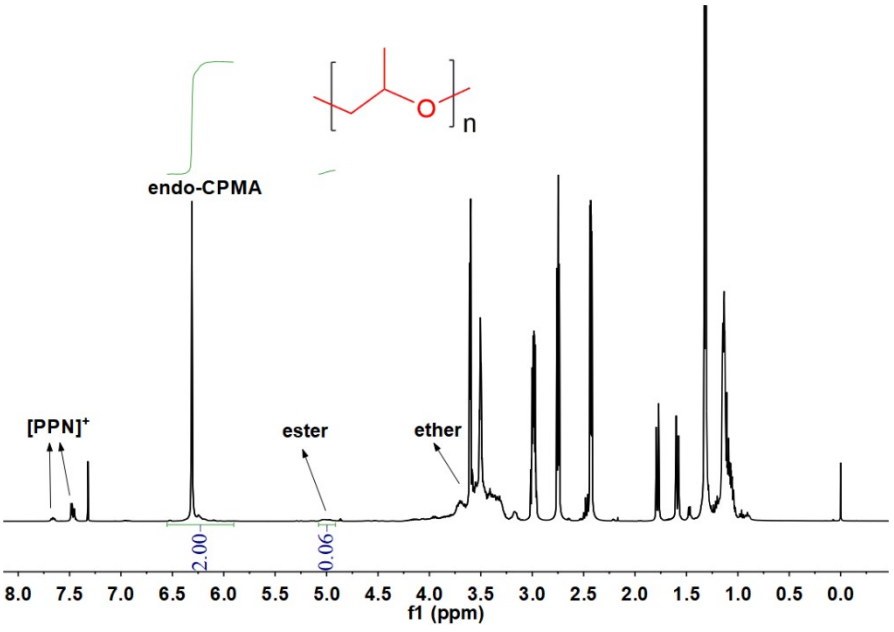

Figure S2. The ^{1}H NMR spectrum of the resulting copolymer catalyzed by $B(C_6F_5)_3$/PPNCl in $CDCl_3$.

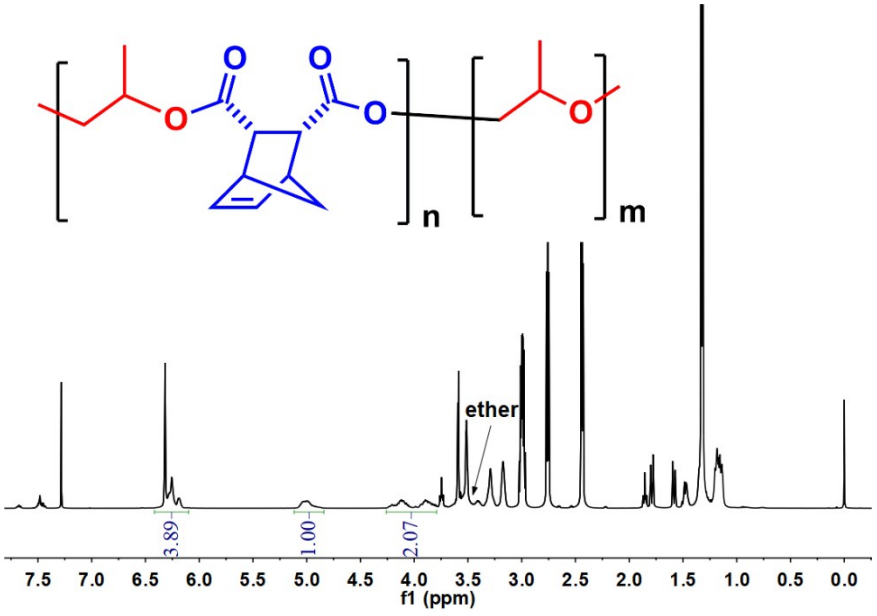

Figure S3. ^{1}H NMR spectrum of the reaction mixture catalyzed by BEt_3/PPNCl with a molar ratio of 2:1 (Conv. = 51%).

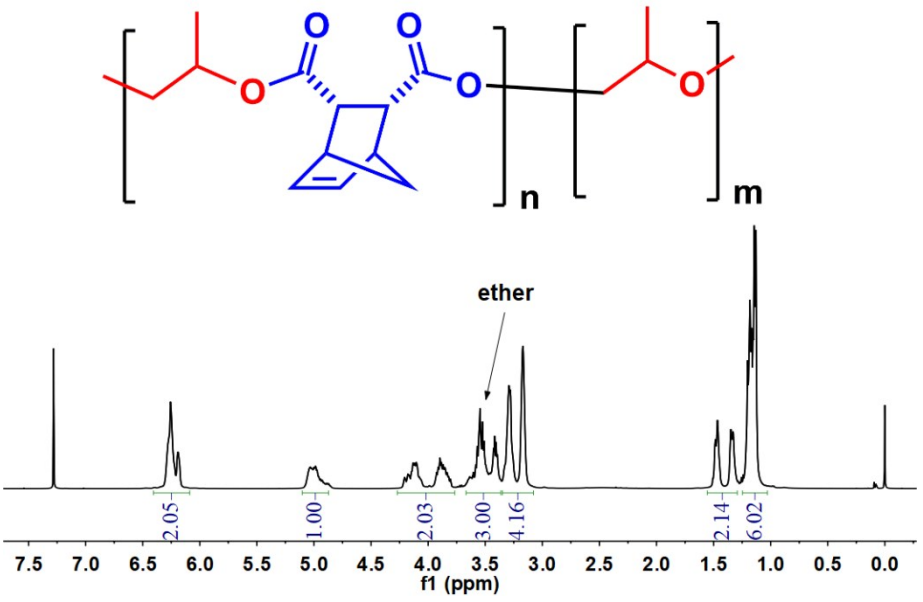

Figure S4. ^{1}H NMR spectrum of the isolated polymer catalyzed by BEt_3/PPNCl with a molar ratio of 2:1 (Conv. = 51%).

4. Determination of regioregularity of polyesters

In the ROAC of anhydrides and asymmetric terminal epoxides, the regioregularity of the polyesters depended on the regioselectivity of the ring-opening of the epoxides. In general, the epoxide is opened at the less sterically hindered methylene carbon, and a regioerror occurs if the epoxide is opened at the methine carbon instead. Because of the S_N2 nature of the ring-opening step, attacking at the methine carbon results into not only a regioerror but also a stereoerror. This means that the regioregularity can be assessed by determining the enantiopurity of polymers synthesized from enantiopure starting materials. Thus, the regioregularity of polyesters was analyzed using chiral gas chromatography after degradation.

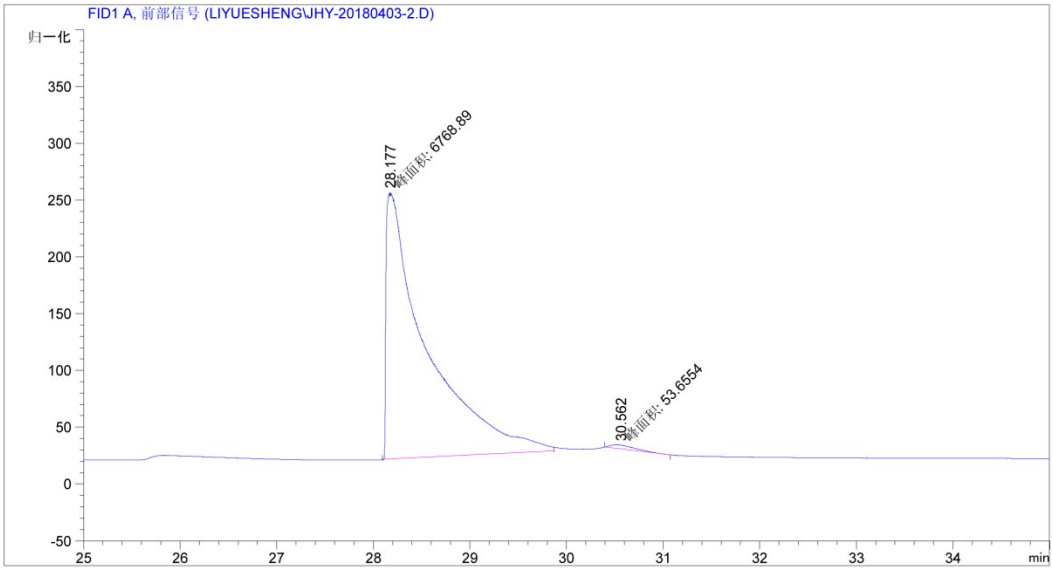

==========

面积百分比报告

==========

排序 : 信号
乘积因子: : 1.0000
稀释因子: : 1.0000
内标使用乘积因子和稀释因子

信号 1: FID1 A, 前部信号

峰 #	保留时间 [min]	类型	峰宽 [min]	峰面积 [pA*s]	峰高 [pA]	峰面积 %
1	28.177	MM	0.4813	6768.88574	234.39037	99.21356
2	30.562	MM	0.2817	53.65545	3.17455	0.78644
总量 :				6822.54119	237.56491	

Figure S5. Chiral GC analysis of the *S*-enriched 1,2-propanediol (*ee* = 98.4%) resulting from the hydrolysis of poly(*endo*-CPMA-*alt*-*S*PO).

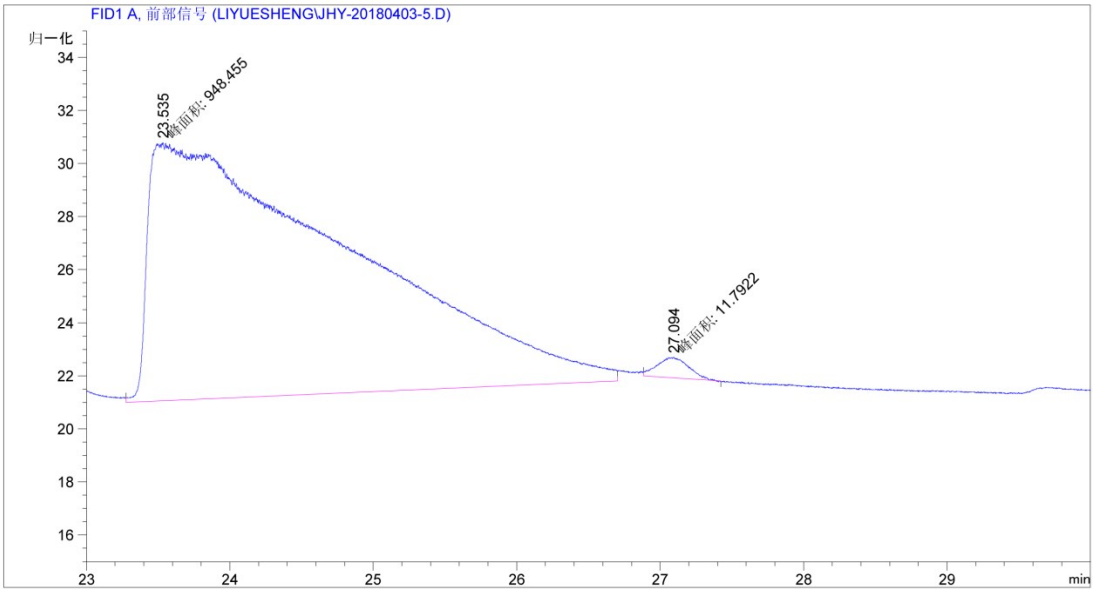

==========

面积百分比报告

==========

排序 : 信号
乘积因子: : 1.0000
稀释因子: : 1.0000
内标使用乘积因子和稀释因子

信号 1: FID1 A, 前部信号

峰 #	保留时间 [min]	类型	峰宽 [min]	峰面积 [pA*s]	峰高 [pA]	峰面积 %
1	23.535	MM	1.6251	948.45544	9.72726	98.77196
2	27.094	MM	0.2536	11.79222	7.74879e-1	1.22804

总量 : 960.24767 10.50214

Figure S6. Chiral GC analysis of the *S*-enriched 1,2-butanediol (*ee* = 97.6%) resulting from the hydrolysis of poly(*endo*-CPMA-*alt*-*S*BO).

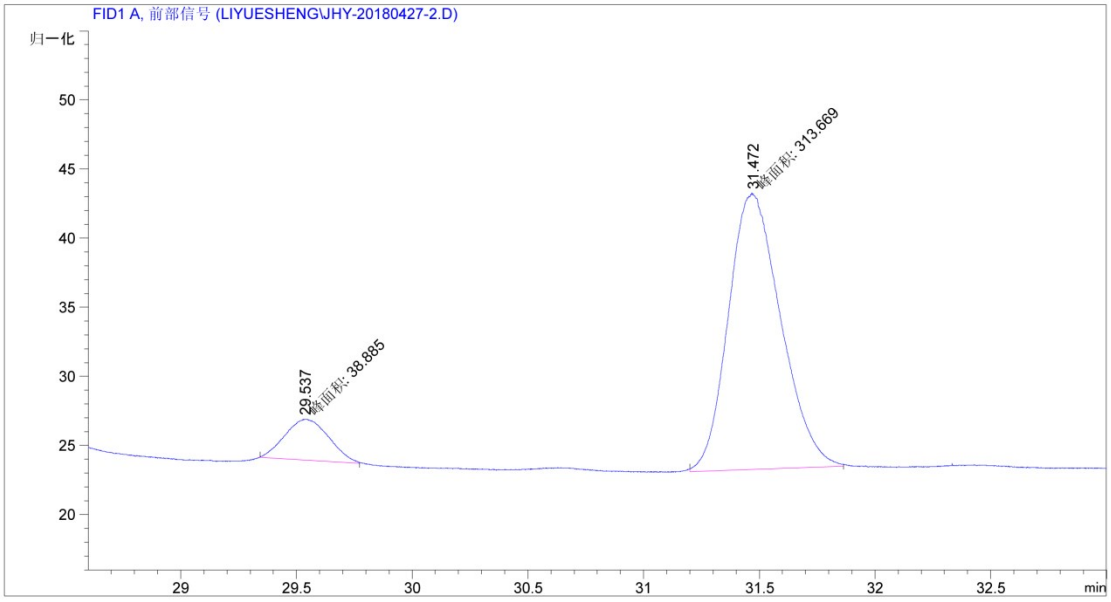

==========

面积百分比报告

==========

排序 : 信号
乘积因子: : 1.0000
稀释因子: : 1.0000
内标使用乘积因子和稀释因子

信号 1: FID1 A, 前部信号

峰 #	保留时间 [min]	类型	峰宽 [min]	峰面积 [pA*s]	峰高 [pA]	峰面积 %
1	29.537	MM	0.2189	38.88505	2.96066	11.02952
2	31.472	MM	0.2621	313.66931	19.94963	88.97048
总量 :				352.55436	22.91029	

Figure S7. Chiral GC analysis of the *S*-enriched Styrene glycol (*ee* = 77.9%) resulting from the hydrolysis of poly(*endo*-CPMA-*alt*-*S*SO).

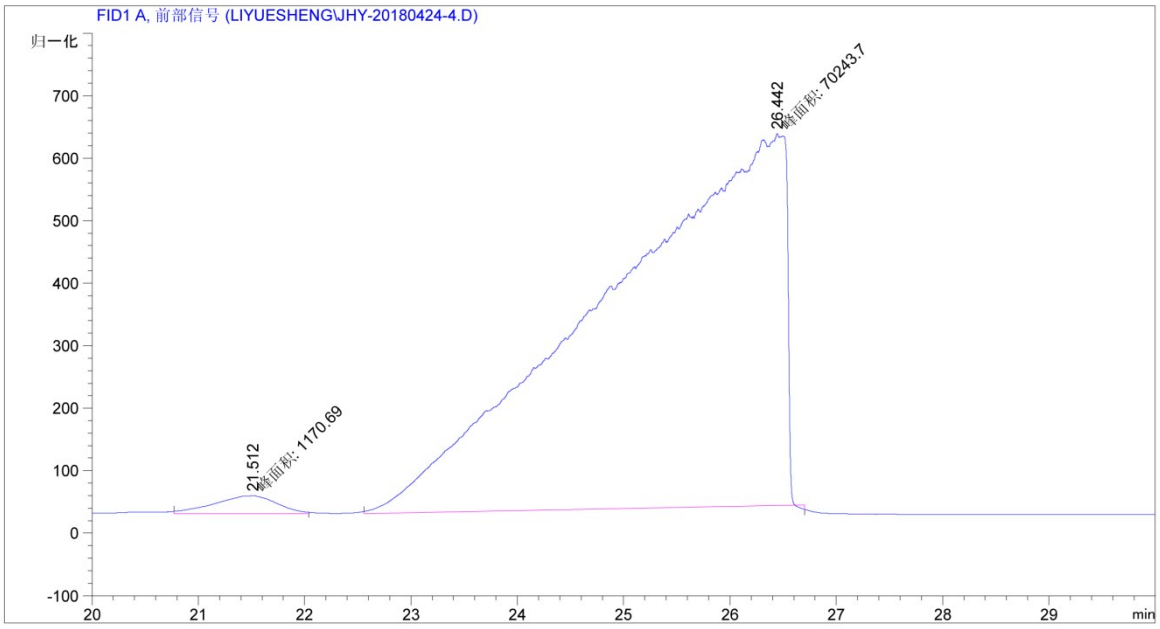

==========

面积百分比报告

==========

排序 : 信号
乘积因子: : 1.0000
稀释因子: : 1.0000
内标使用乘积因子和稀释因子

信号 1: FID1 A, 前部信号

峰 #	保留时间 [min]	类型	峰宽 [min]	峰面积 [pA*s]	峰高 [pA]	峰面积 %
1	21.512	MM	0.6713	1170.68921	29.06328	1.63929
2	26.442	MM	1.9684	7.02437e4	594.76257	98.36071

总量 : 7.14143e4 623.82586

Figure S8. Chiral GC analysis of the *S*-enriched 3-Benzyloxy-1,2-propanediol (*ee* = 96.8%) resulting from the hydrolysis of poly(*endo*-CPMA-*alt*-*S*BGE).

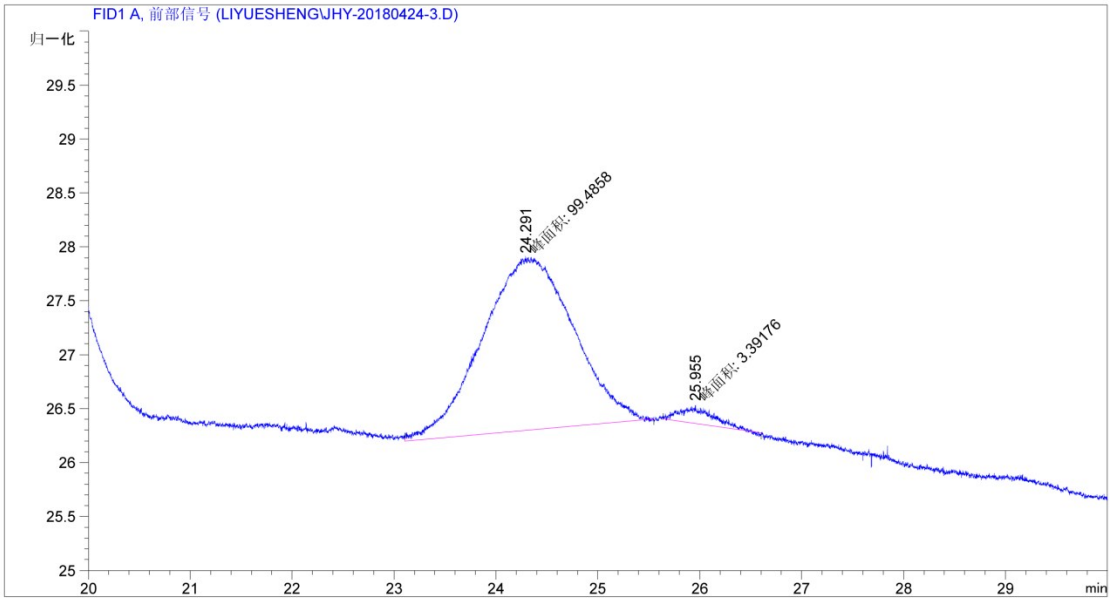

==========

面积百分比报告

==========

排序 : 信号
乘积因子: : 1.0000
稀释因子: : 1.0000
内标使用乘积因子和稀释因子

信号 1: FID1 A, 前部信号

峰 #	保留时间 [min]	类型	峰宽 [min]	峰面积 [pA*s]	峰高 [pA]	峰面积 %
1	24.291	MM	1.0348	99.48579	1.60226	96.70311
2	25.955	MM	0.3337	3.39176	1.69419e-1	3.29689
总量 :				102.87755	1.77168	

Figure S9. Chiral GC analysis of the *S*-enriched 3-Phenoxy-1,2-propanediol (*ee* = 93.4%) resulting from the hydrolysis of poly(*endo*-CPMA-*alt*-*S*PGE).

5. Kinetic Resolution Experiment with *endo*-CPMA and PO using BEt_3/PPNCl

A kinetic resolution experiment of PO was attempted by the ROAC of CPMA with racemic PO catalyzed by BEt_3/PPNCl. The copolymerization was carried out at 80 ºC with the molar ratio of [BEt_3]/[PPNCl]/[*endo*-CPMA]/[*rac*-PO] = 1:1:100:500. After 80 min, 18.4% PO was inserted into polymers according to the calculating conversion of *endo*-CPMA. Chiral GC analysis indicated that the *ee* of propylene glycol degrading from the resultant polyester was 4.2% *S*-enriched. Based on the equation (1), relative rate constant k_{rel} was determined to be 1.52, demonstrating that S-PO was preferentially consuming in contrast to *R*-PO in the *rac*-PO.

$$k_{rel} = \ln[(1\text{-conv.})(1\text{-}ee)]/\ln[(1\text{-conv.})(1+ee)] \qquad (1)$$

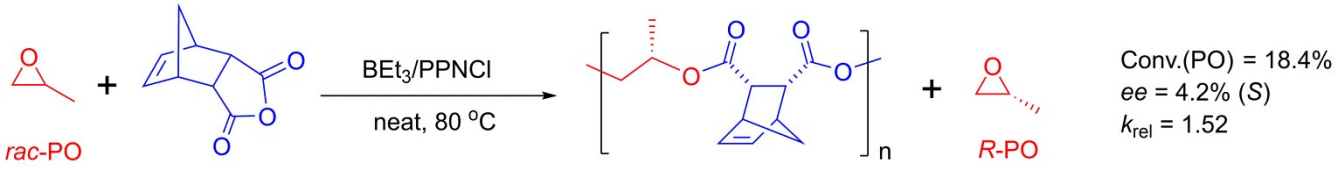

Scheme S1. Kinetic resolution of PO by the ROAC with *endo*-CPMA using organocatalyst.

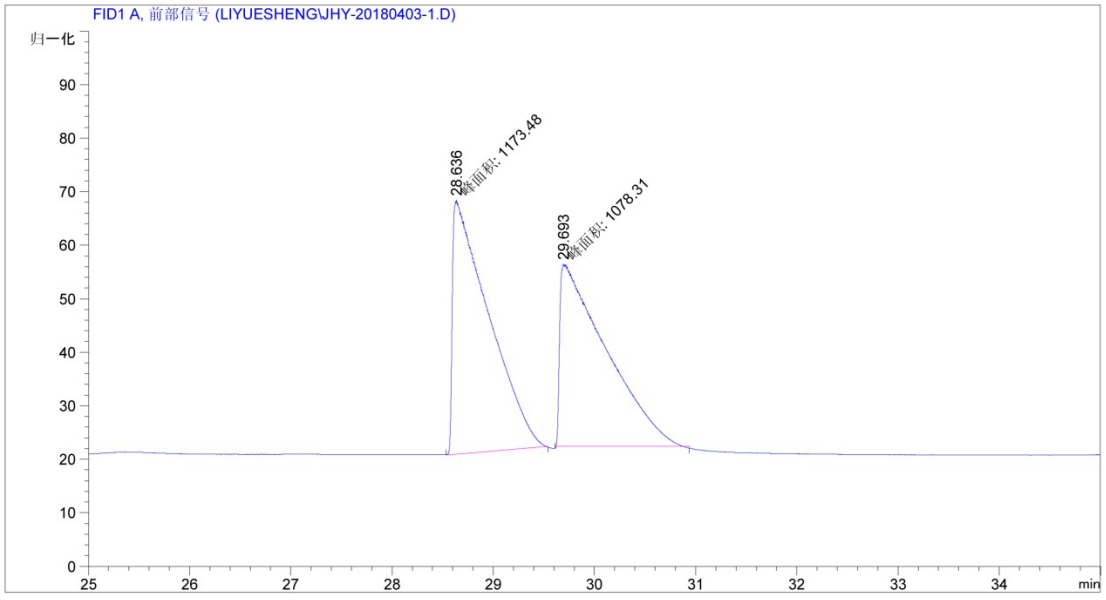

==========

面积百分比报告

==========

排序 : 信号
乘积因子: : 1.0000
稀释因子: : 1.0000
内标使用乘积因子和稀释因子

信号 1: FID1 A, 前部信号

峰 #	保留时间 [min]	类型	峰宽 [min]	峰面积 [pA*s]	峰高 [pA]	峰面积 %
1	28.636	MM	0.4119	1173.48096	47.47739	52.11322
2	29.693	MM	0.5271	1078.31055	34.09282	47.88678
总量 :				2251.79150	81.57021	

Figure S10. Chiral GC analysis of the resultant 1,2-propanediol (*ee* = 4.2%) resulting from the hydrolysis of poly(*endo*-CPMA-*alt*-*rac*PO).

6. Determination of stereoregularity of diester units

The different stereostructure of diester units in the polyesters could be illuminated by ^{1}H, ^{13}C and gradient HSQC NMR spectroscopy. Taking poly(*endo*-CPMA-*alt*-PO) for example, the *cis* stereochemical content of diesters was calculated by integrating the resonance peaks of *trans* α-protons at 2.70 ppm and the signals from 3.41 to 3.17 ppm (see Figure S11). Notably, the signals at 3.41-3.17 ppm include methine regions belonging to norbornene ring. As the matter of fact, if the proton at 5.0 ppm was normalized, the integral area of the resonance peaks at 2.70 ppm is on behalf of the *trans*-proton content. The absence of *trans*-diester at 2.70 ppm indicates that BEt_3/PPNCl is unable to catalyze the epimerization of diester stereochemistry after reaching high or complete conversion of CPMA under the conditions described for Table 1. Meanwhile, ^{13}C and HSQC NMR spectra further prove the conclusion. Although the cis stereochemistry of diester units was retained, the tricyclic anhydrides were regiorandom insertion in the ROAC. There are another two stereochemical possibilities of norbornenyl ring for the incorporation of *endo*-CPMA except the diester units. Thus, this polymerization process retained the *cis*-stereochemistry of the tricyclic anhydrides. However, the incorporation of the diester units was still stereoirregular because the process did not desymmetrize these *meso*-tricyclic anhydrides.

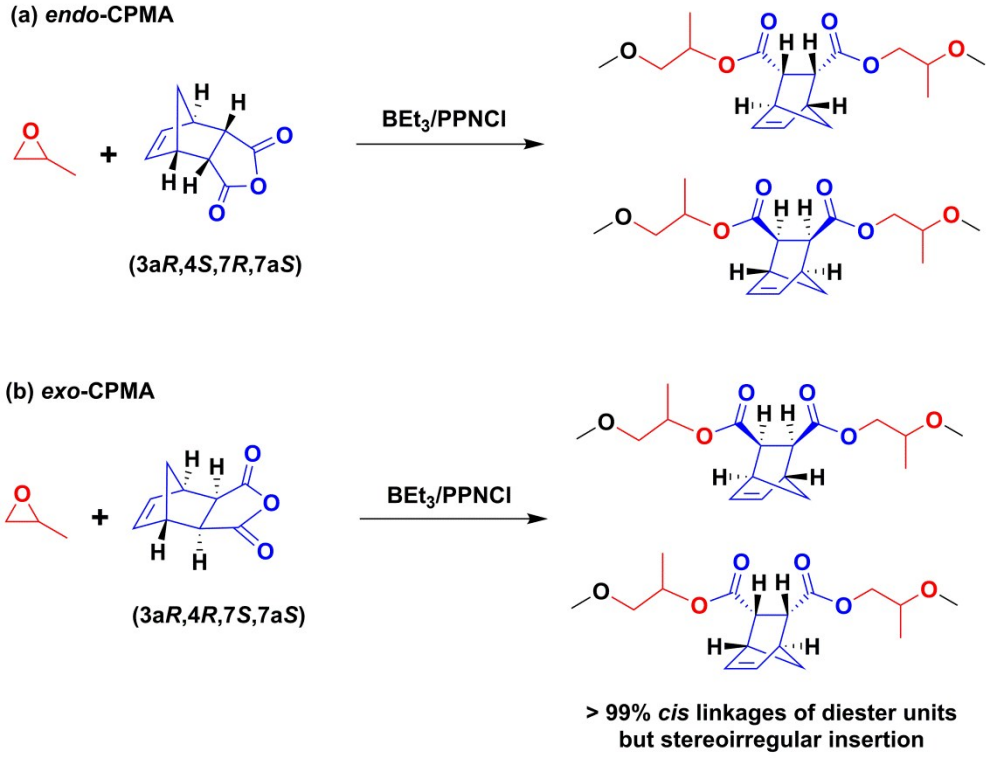

Scheme S2. Stereochemical possibilities for the copolymerization of PO and CPMA, in which the ring-opening of PO is regioselective.

7. GPC evolution plots

The purity of anhydrides had a profound impact on the molecular weights and molecular weight distributions (MWDs) of the corresponding polyesters. When anhydrides were used as received, the bimodal and wide MWDs were detected GPC analyses (Figure S5). While unimodal and narrow MWDs were available if anhydrides used were purified three times by the way of sublimation. The results implied that the presence of adventitious water or trace amounts of hydrolysed anhydride acted as a bifunctional chain transfer agent. The bifunctional agents were expected to propagate at a similar rate as chains initiated from the catalysts, leading to chain growth from both hydroxyl moieties. Therefore, a bimodal distribution was observed from the GPC curve.

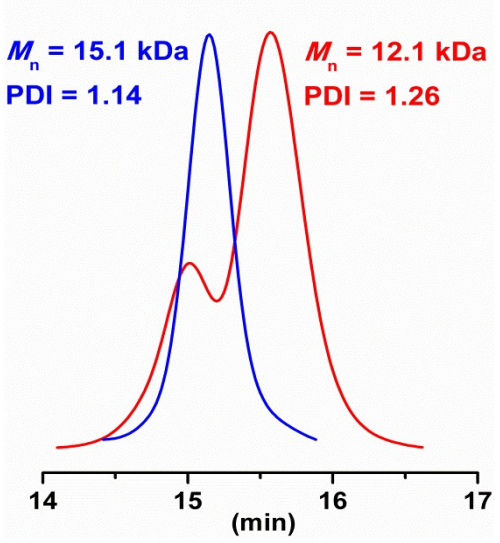

Figure S11. The GPC curves of the corresponding polyesters from unrefined and sublimed (× 3) *endo*-CPMA.

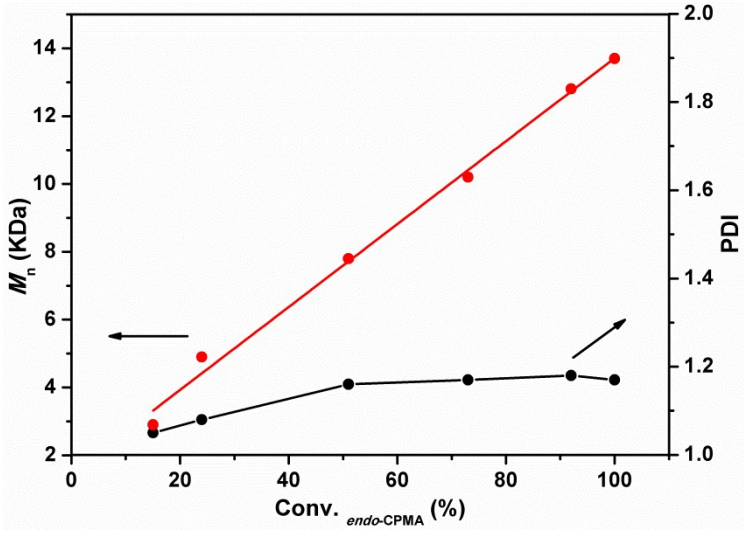

Figure S12. Plots of M_n and PDI versus *endo*-CPMA conversion for the alternating copolymerization with an excess of PO.

8. Gradient HSQC NMR spectra of the resultant polyesters

The two-dimentional HSQC NMR spectra of stereoregular and stereoirregular poly(CPMA-*alt*-PO) were shown as described below. Owing to the complete elimination of epimerization by introducing one equivalent of BEt_3, well-defined and *cis*-enriched polyesters were synthesized.

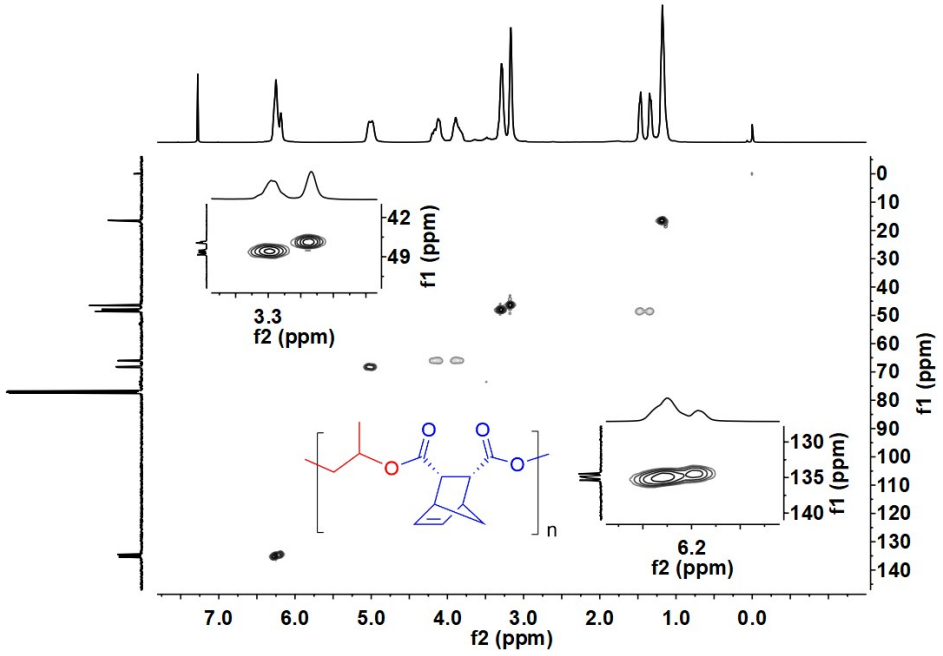

Figure S13. The gradient HSQC NMR spectra of stereoregular poly(*endo*-CPMA-*alt*-PO) catalyzed by single BEt_3/PPNCl with complete suppression of epimerization.

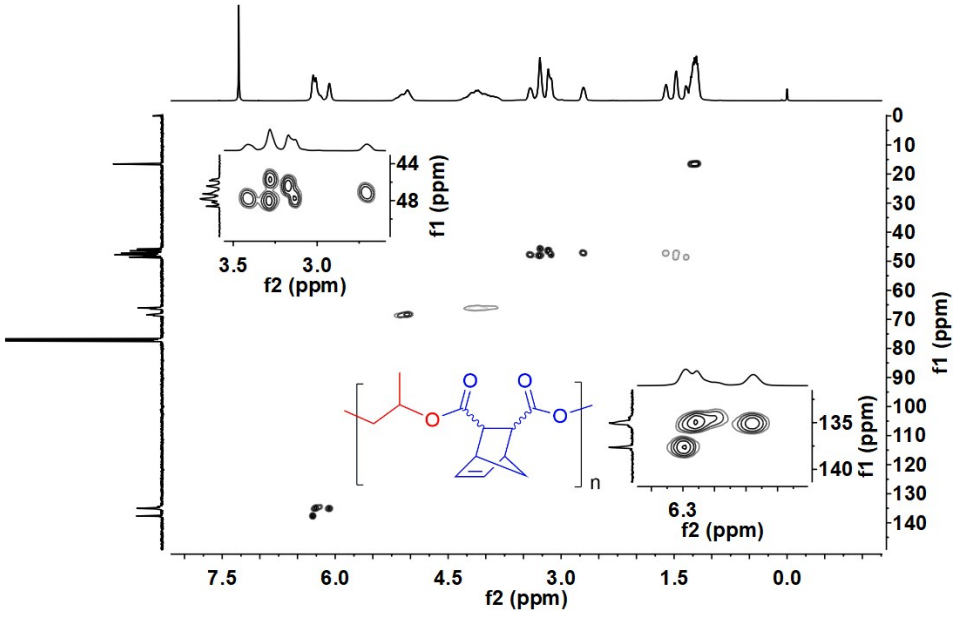

Figure S14. The gradient HSQC NMR spectra of stereoirregular poly(*endo*-CPMA-*alt*-PO) catalyzed by single PPNCl because of epimerization.

9. NMR spectra of block copolyesters

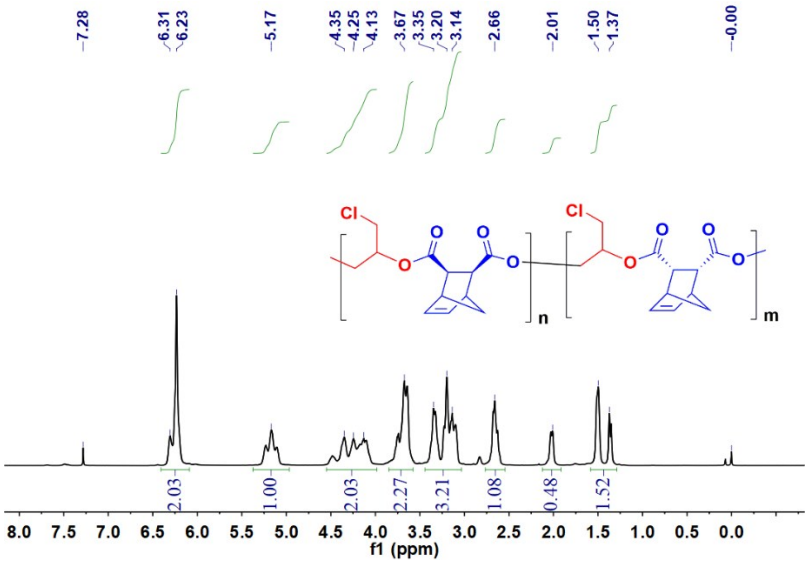

Figure S15. ^{1}H NMR spectrum of the block copolymer of poly(*endo*-CPMA-*alt*-ECH) and poly(*exo*-CPMA- *alt*-ECH) in $CDCl_3$.

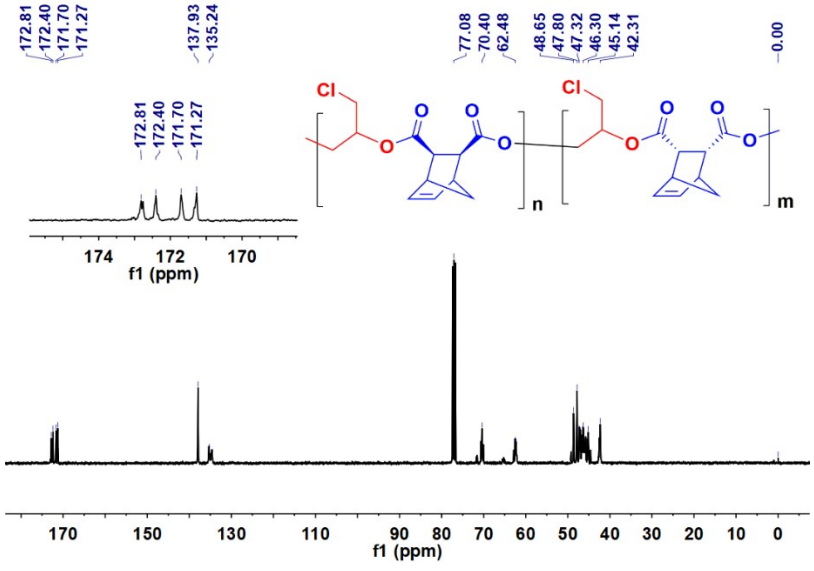

Figure S16. ^{13}C NMR spectrum of the block copolymer of poly(*endo*-CPMA-*alt*-ECH) and poly(*exo*-CPMA-*alt*-ECH) in $CDCl_3$.

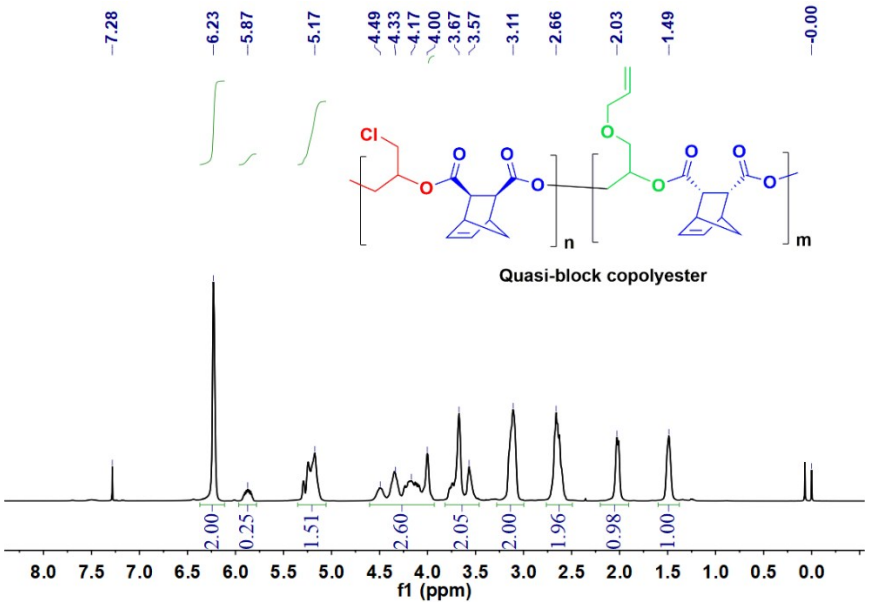

Figure S17. ^{1}H NMR spectrum of the quasi-block copolymer of poly(*exo*-CPMA-*alt*-ECH) and poly(*exo*-CPMA-*alt*-AGE) in $CDCl_3$.

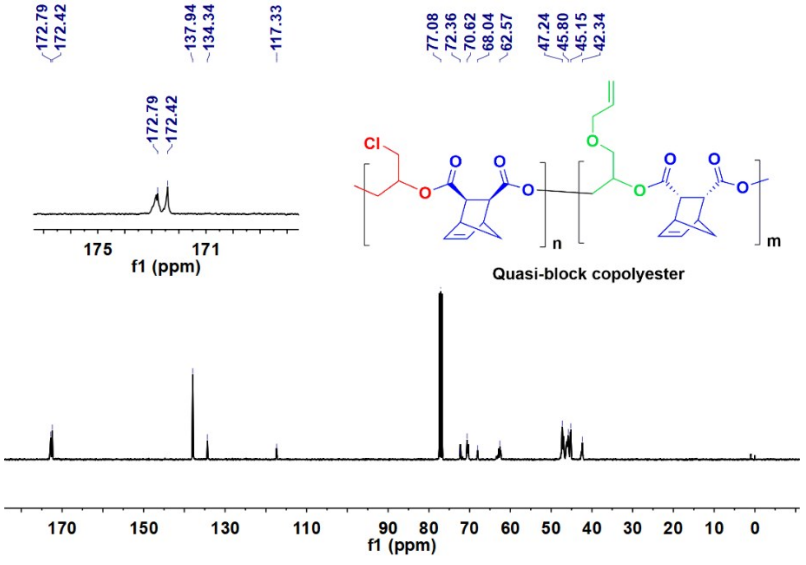

Figure S18. ^{13}C NMR spectrum of the quasi-block copolymer of poly(*exo*-CPMA-*alt*-ECH) and poly(*exo*-CPMA-*alt*-AGE) in $CDCl_3$.

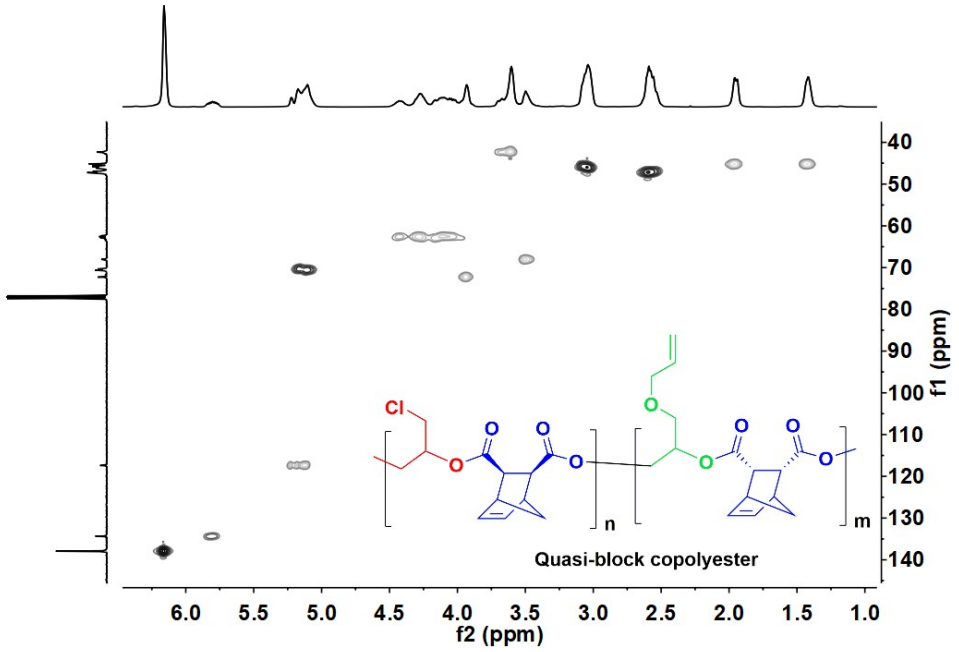

Figure S19. The gradient HSQC NMR spectrum of the quasi-block copolymer of poly(*exo*-CPMA-*alt*-ECH) and poly(*exo*-CPMA-*alt*-AGE) in $CDCl_3$.

10. Representative ^{1}H and ^{13}C NMR spectra of polyesters

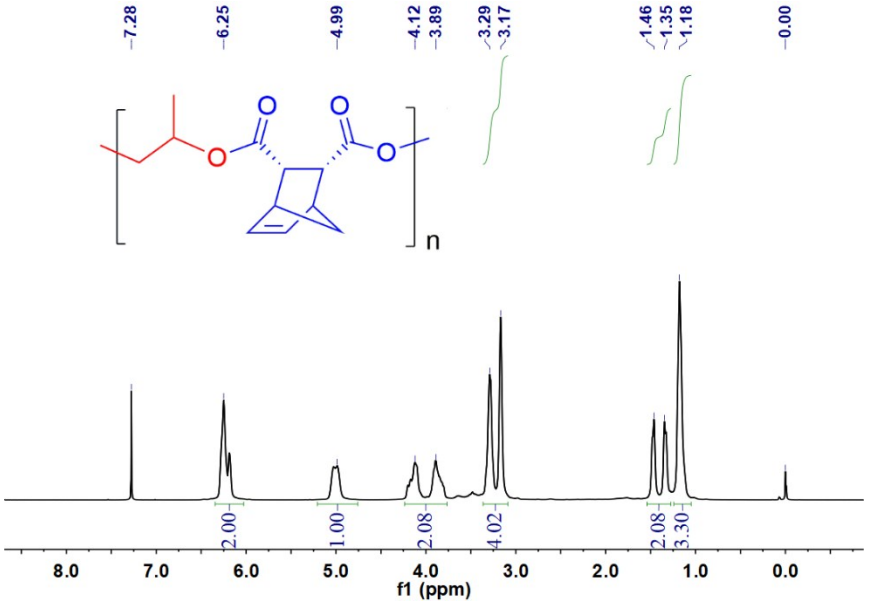

Figure S20. ^{1}H NMR spectrum of the stereoregular poly(*endo*-CPMA-*alt*-PO) (*cis* > 99%) in $CDCl_3$.

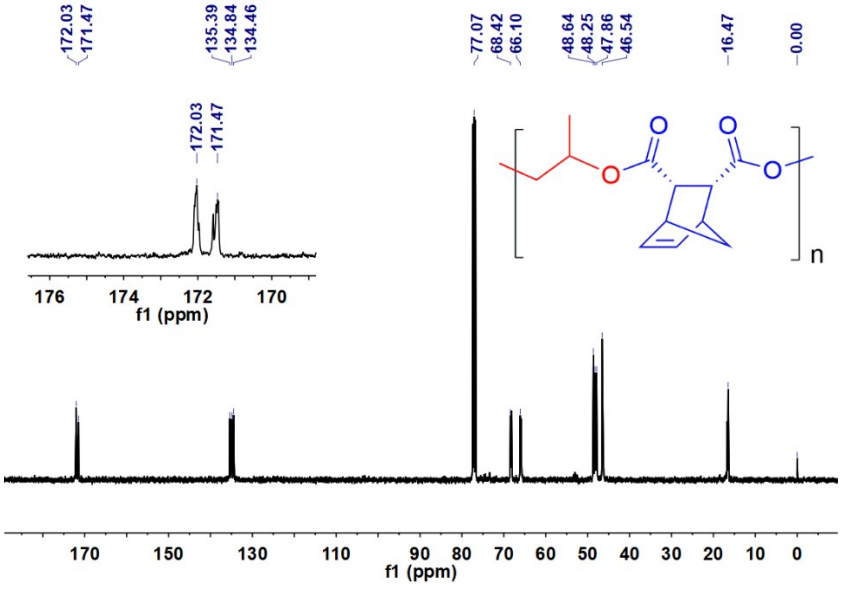

Figure S21. ^{13}C NMR spectrum of the stereoregular poly(*endo*-CPMA-*alt*-PO) (*cis* > 99%) in $CDCl_3$.

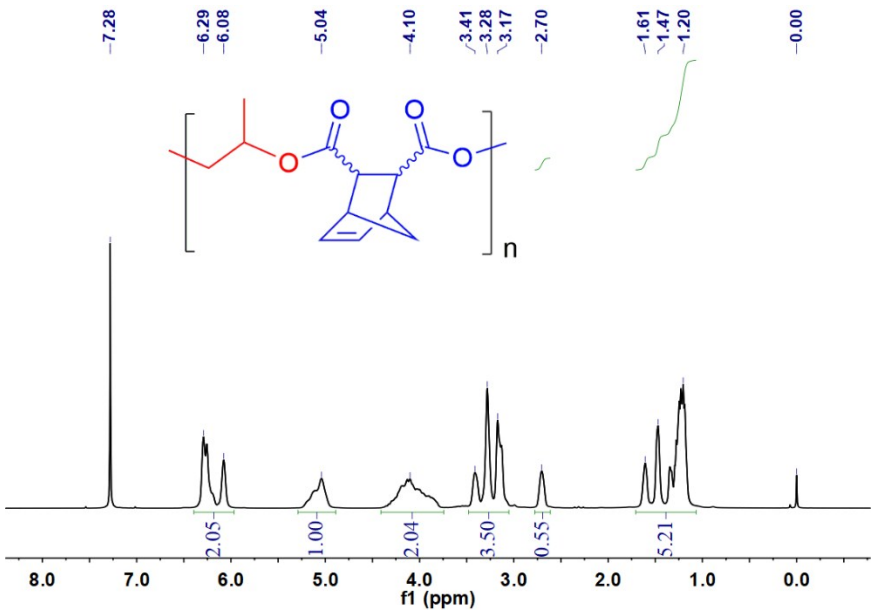

Figure S22. ^{1}H NMR spectrum of the stereoirregular poly(*endo*-CPMA-*alt*-PO) (*cis* = 45%) in $CDCl_3$.

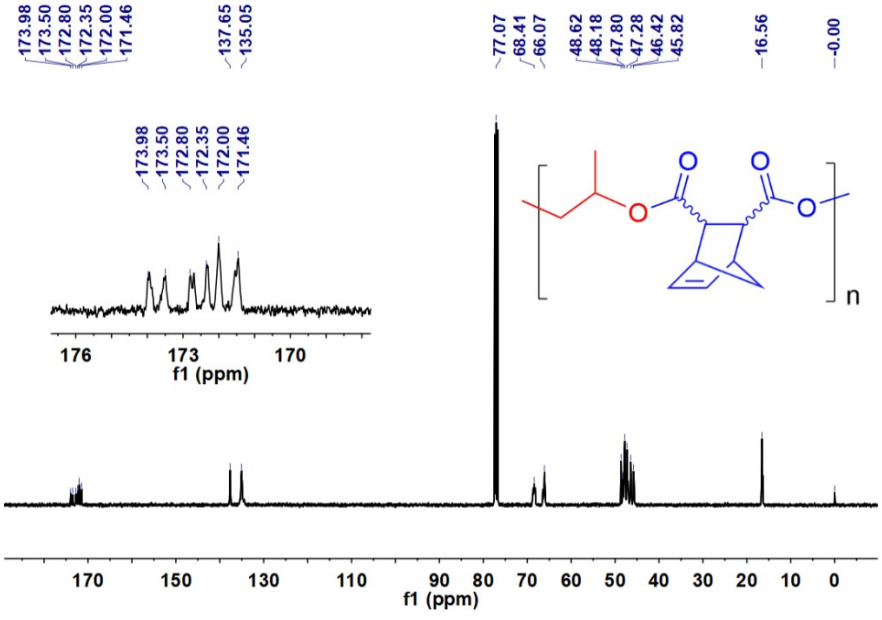

Figure S23. ^{13}C NMR spectrum of the stereoirregular poly(*endo*-CPMA-*alt*-PO) (*cis* = 45%) in $CDCl_3$.

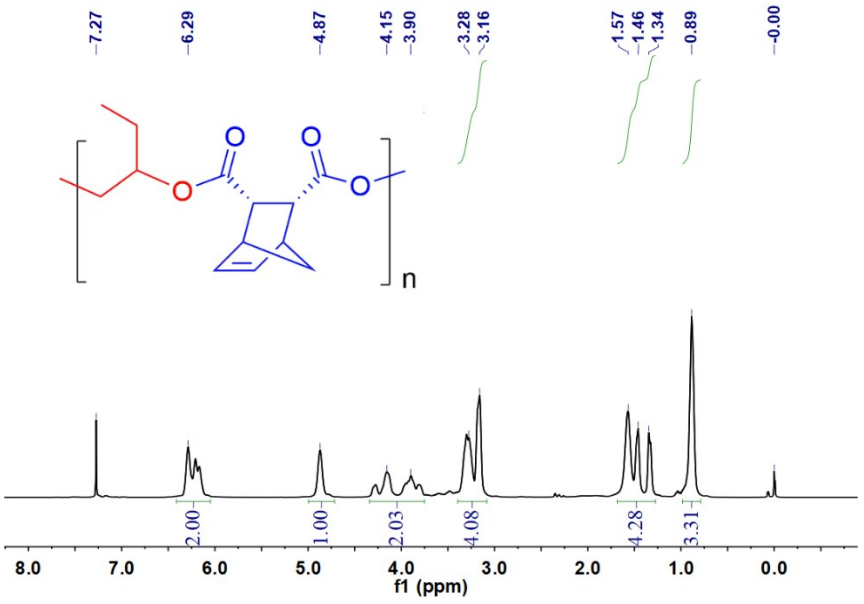

Figure S24. ^{1}H NMR spectrum of the stereoregular poly(*endo*-CPMA-*alt*-BO) (*cis* > 99%) in $CDCl_3$.

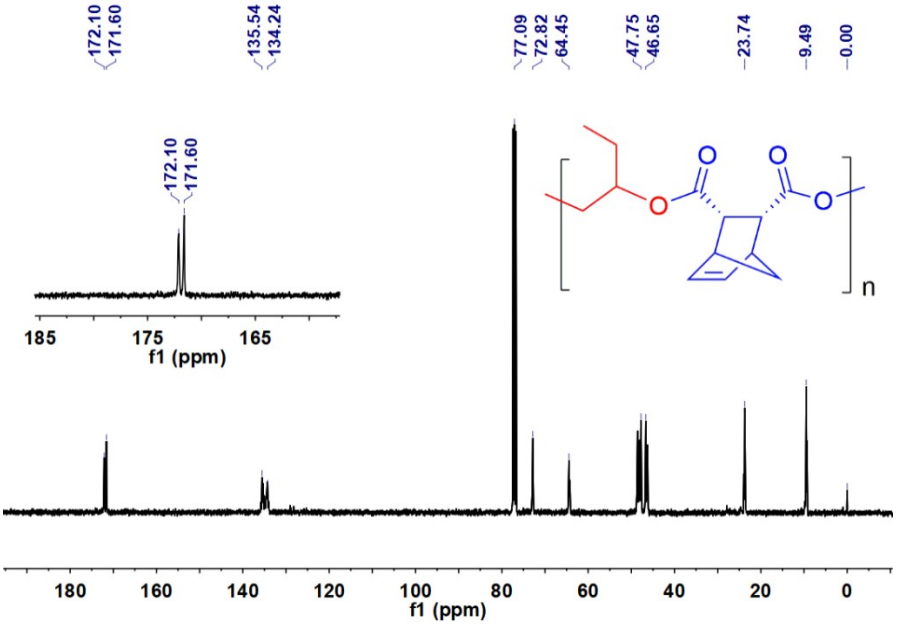

Figure S25. ^{13}C NMR spectrum of the stereoregular poly(*endo*-CPMA-*alt*-BO) (*cis* > 99%) in $CDCl_3$.

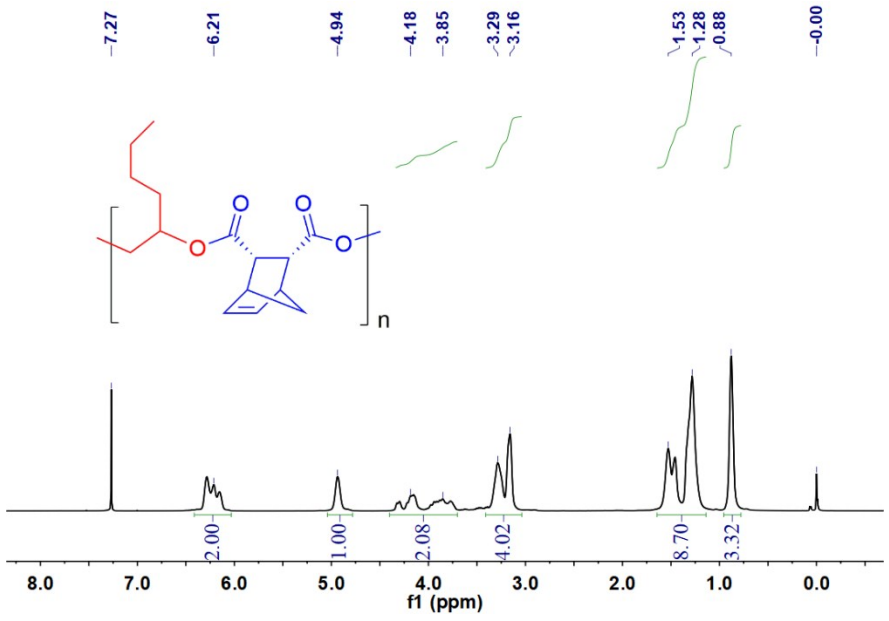

Figure S26. [1]H NMR spectrum of the stereoregular poly(*endo*-CPMA-*alt*-HO) (*cis* > 99%) in $CDCl_3$.

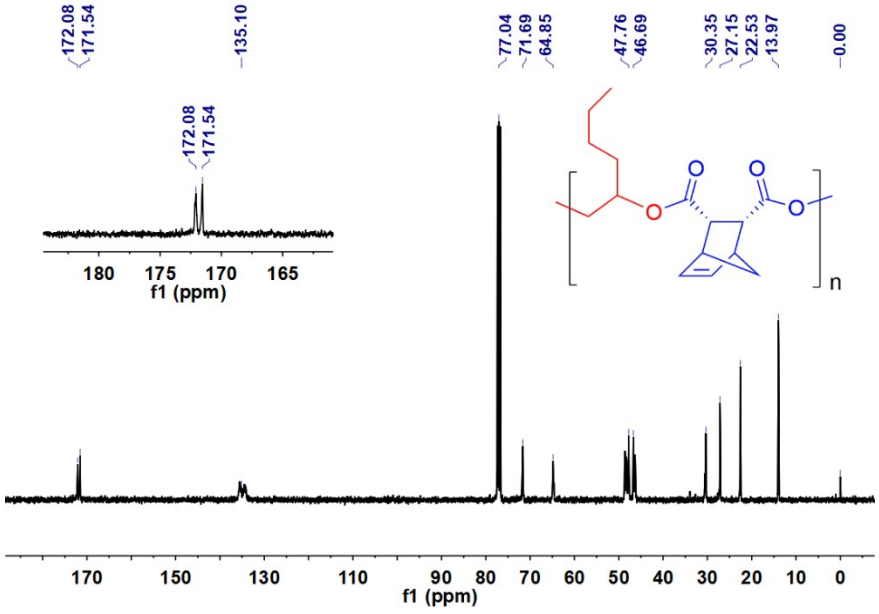

Figure S27. [13]C NMR spectrum of the stereoregular poly(*endo*-CPMA-*alt*-HO) (*cis* > 99%) in $CDCl_3$.

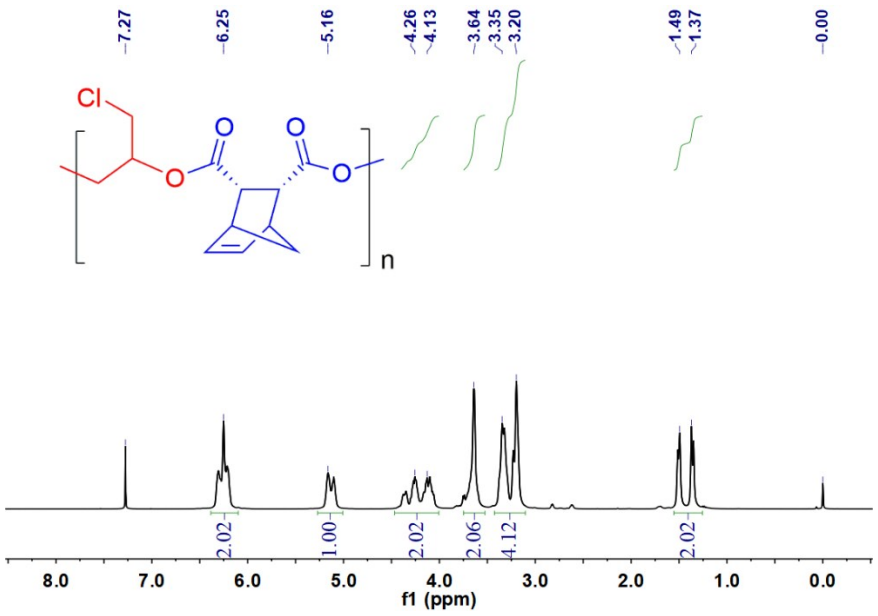

Figure S28. ^{1}H NMR spectrum of the stereoregular poly(*endo*-CPMA-*alt*-ECH) (*cis* > 99%) in $CDCl_3$.

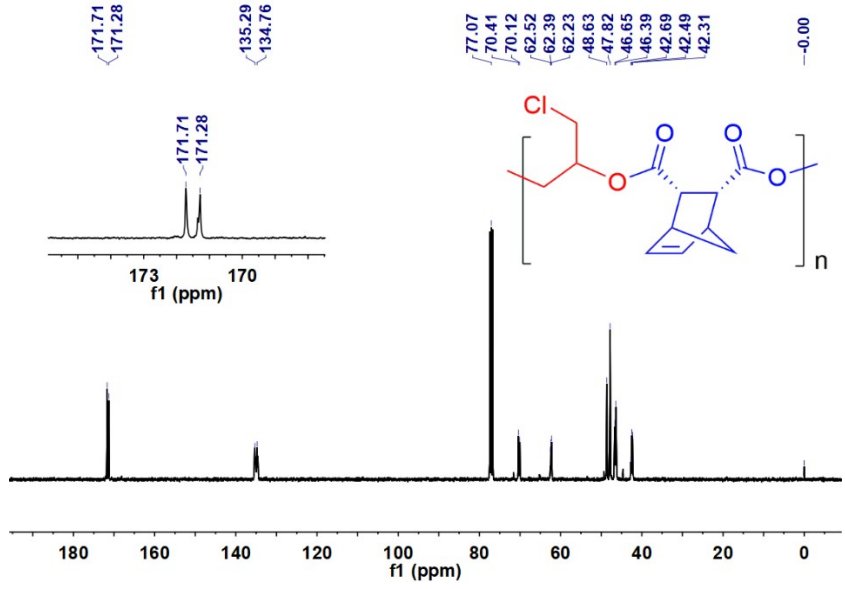

Figure S29. ^{13}C NMR spectrum of the stereoregular poly(*endo*-CPMA-*alt*-ECH) (*cis* > 99%) in $CDCl_3$.

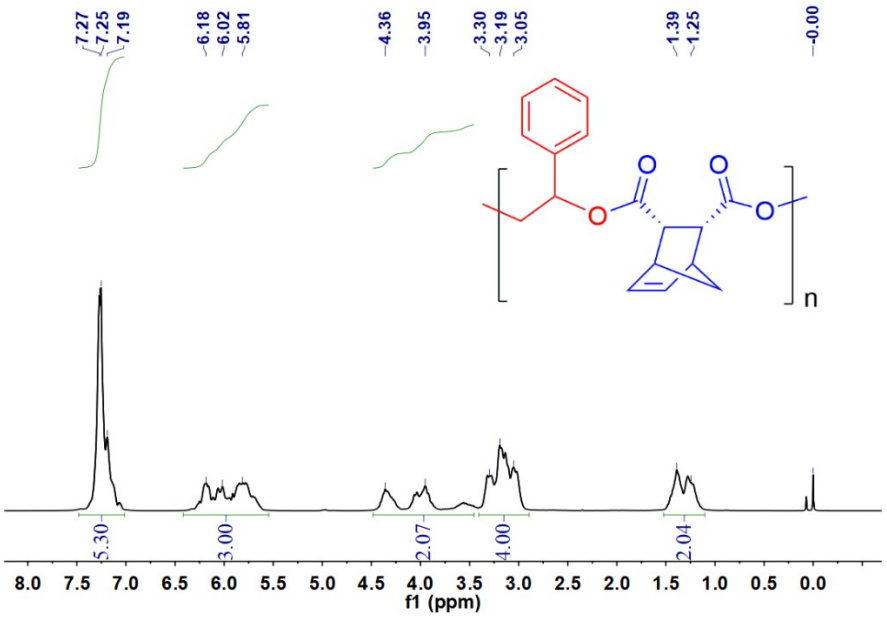

Figure S30. ^{1}H NMR spectrum of the stereoregular poly(*endo*-CPMA-*alt*-SO) (*cis* > 99%) in $CDCl_3$.

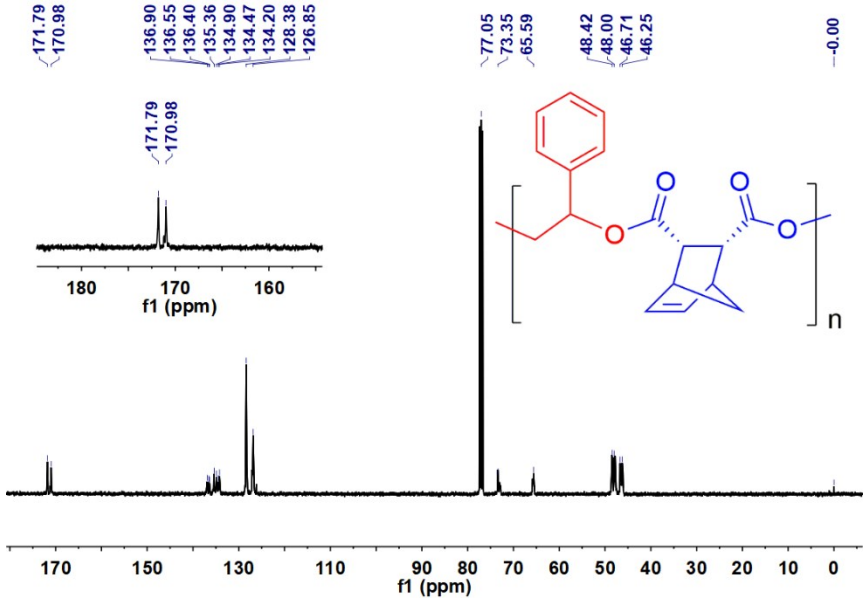

Figure S31. ^{13}C NMR spectrum of the stereoregular poly(*endo*-CPMA-*alt*-SO) (*cis* > 99%) in $CDCl_3$.

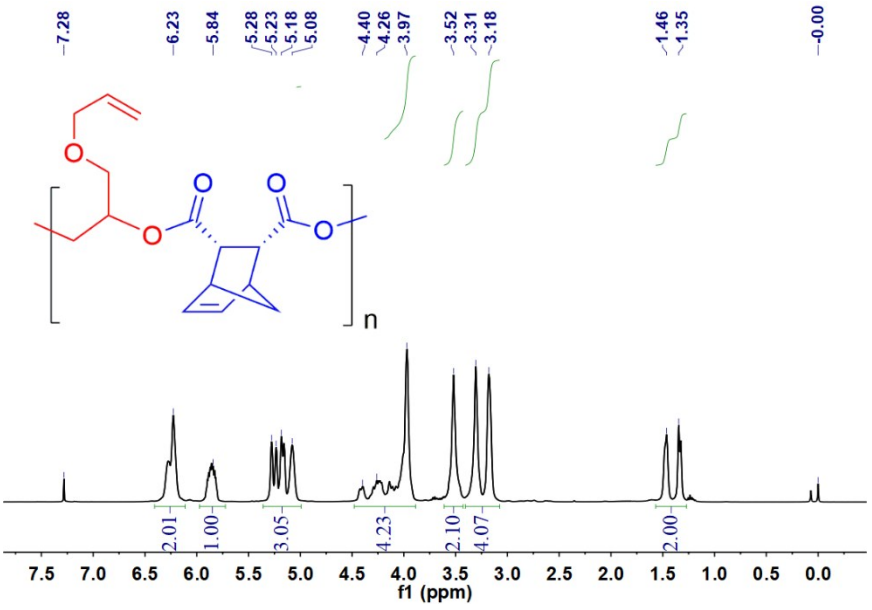

Figure S32. ^{1}H NMR spectrum of the stereoregular poly(*endo*-CPMA-*alt*-AGE) (*cis* > 99%) in $CDCl_3$.

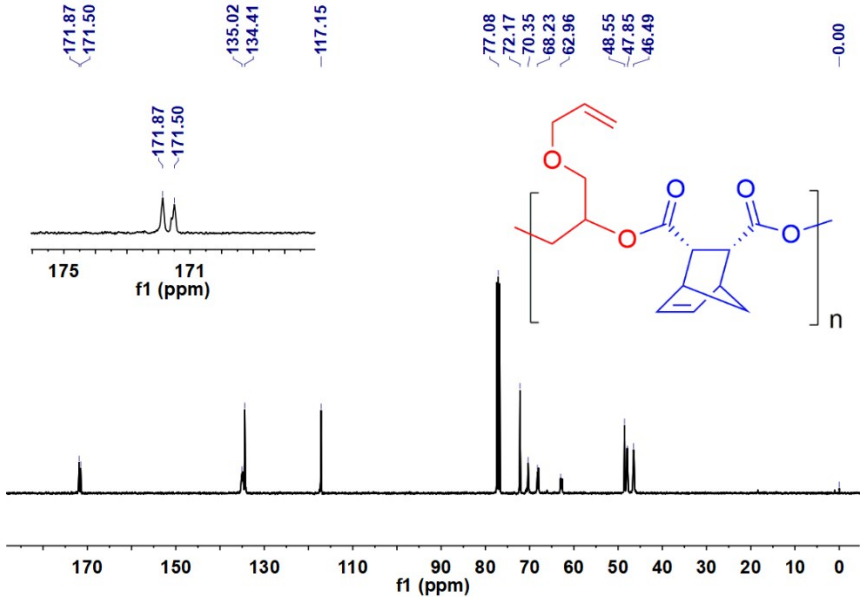

Figure S33. ^{13}C NMR spectrum of the stereoregular poly(*endo*-CPMA-*alt*-AGE) (*cis* > 99%) in $CDCl_3$.

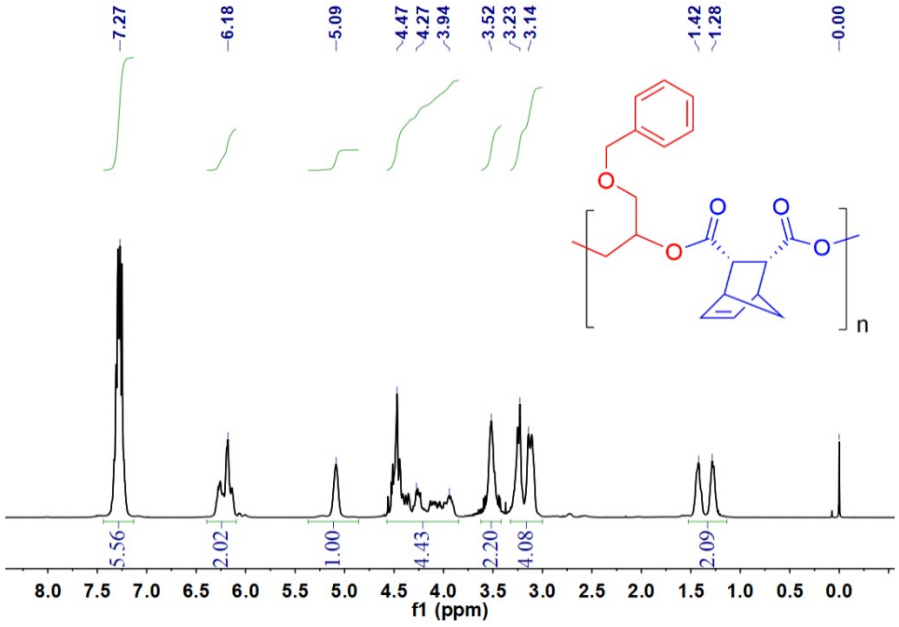

Figure S34. ^{1}H NMR spectrum of the stereoregular poly(*endo*-CPMA-*alt*-BGE) (*cis* > 99%) in $CDCl_3$.

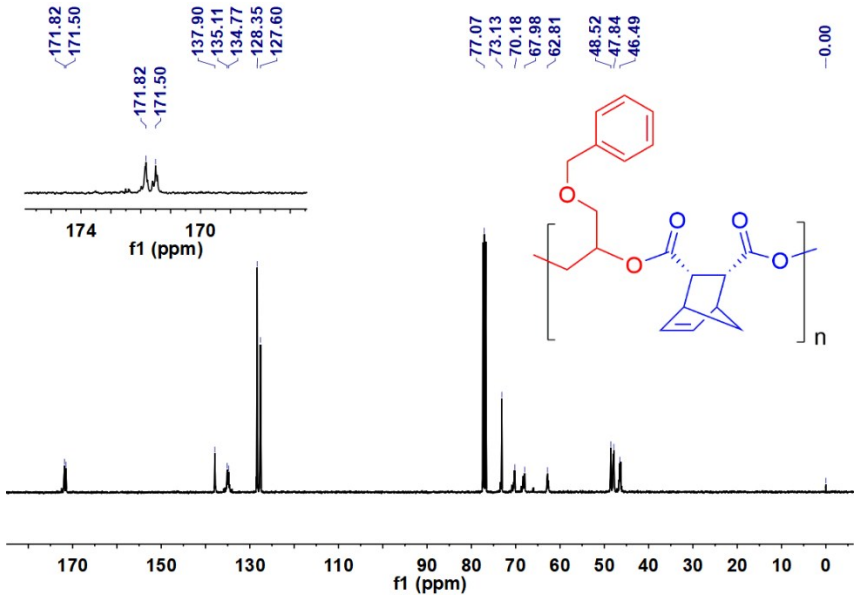

Figure S35. ^{13}C NMR spectrum of the stereoregular poly(*endo*-CPMA-*alt*-BGE) (*cis* > 99%) in $CDCl_3$.

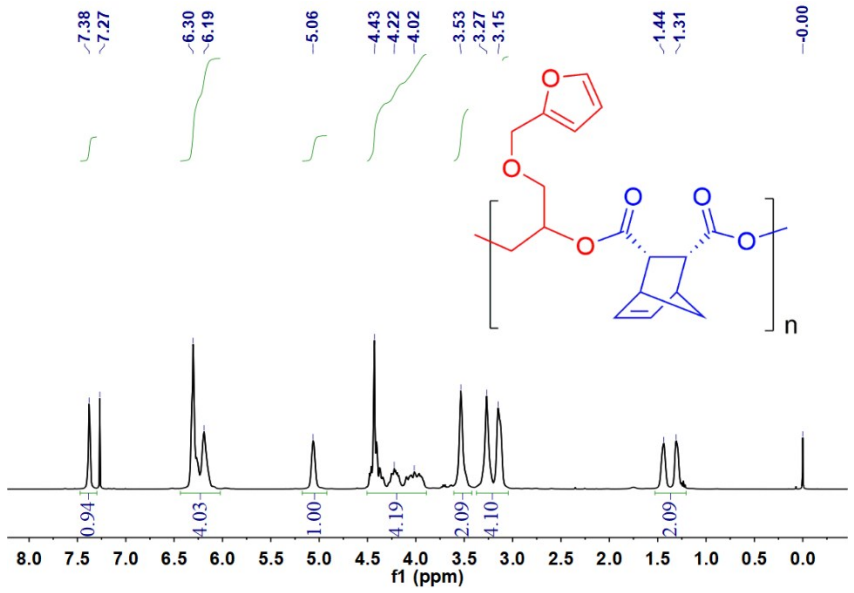

Figure S36. ^{1}H NMR spectrum of the stereoregular poly(*endo*-CPMA-*alt*-FGE) (*cis* > 99%) in $CDCl_3$.

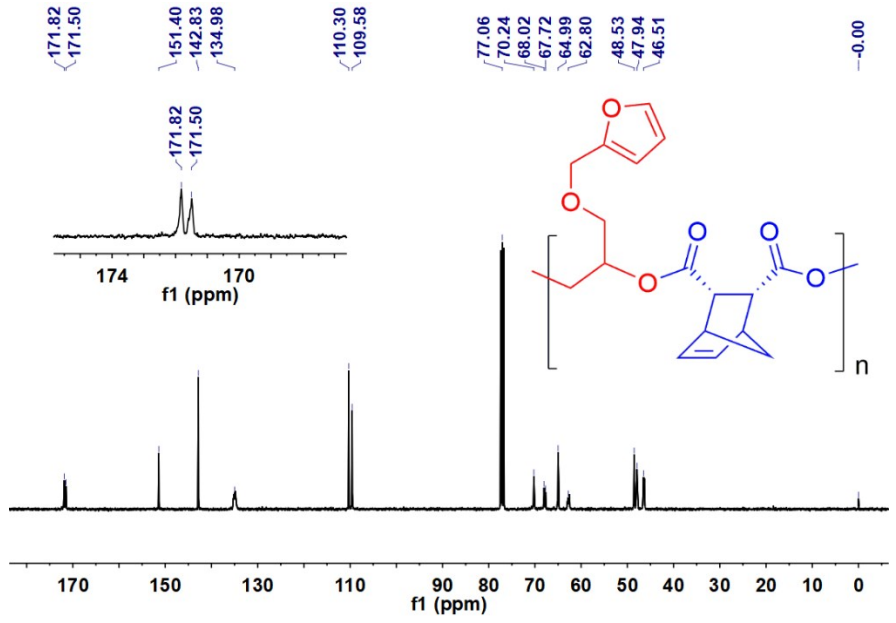

Figure S37. ^{13}C NMR spectrum of the stereoregular poly(*endo*-CPMA-*alt*-FGE) (*cis* > 99%) in $CDCl_3$.

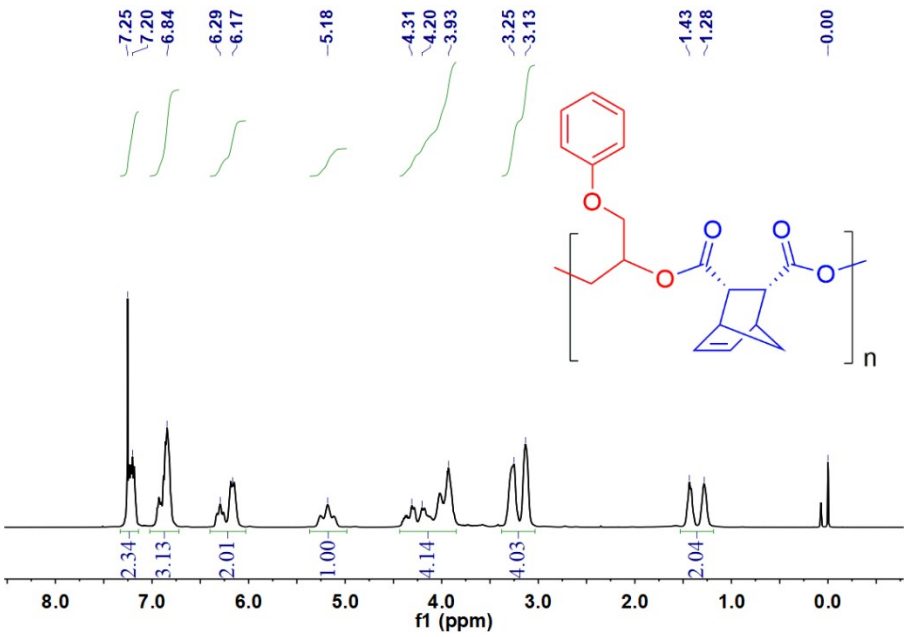

Figure S38. ^{1}H NMR spectrum of the stereoregular poly(*endo*-CPMA-*alt*-PGE) (*cis* > 99%) in $CDCl_3$.

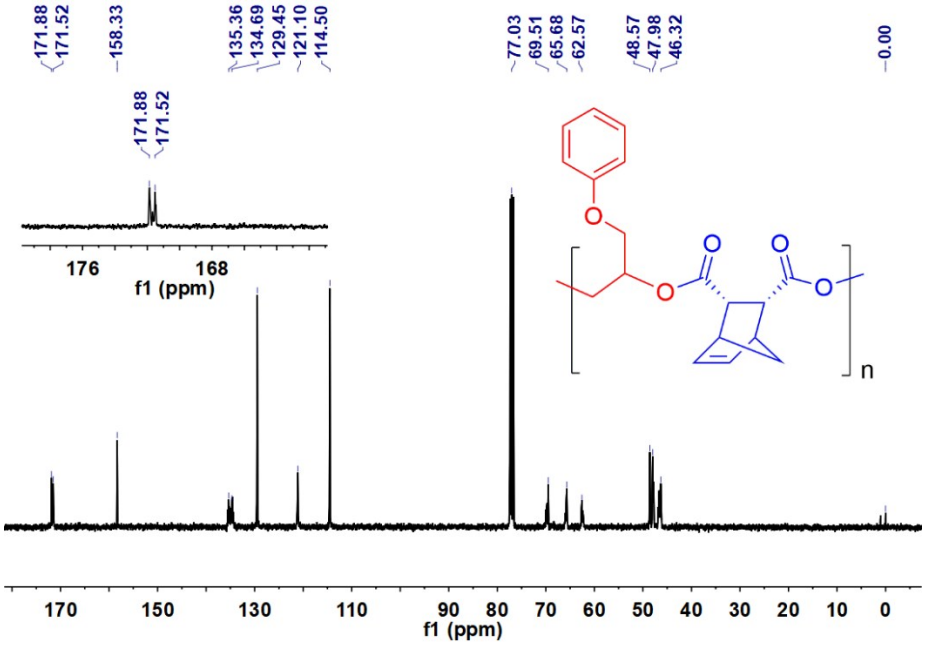

Figure S39. ^{13}C NMR spectrum of the stereoregular poly(*endo*-CPMA-*alt*-PGE) (*cis* > 99%) in $CDCl_3$.

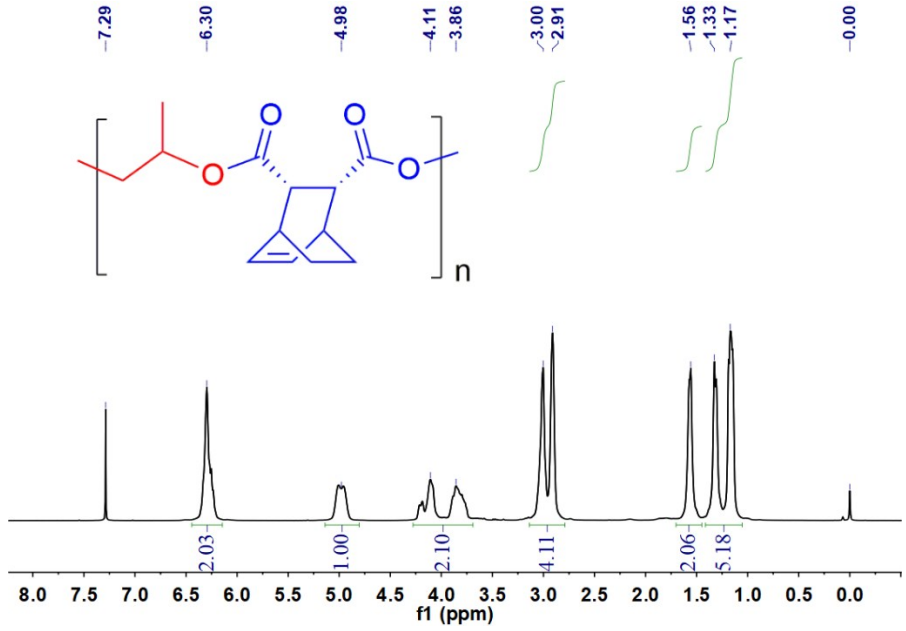

Figure S40. [1]H NMR spectrum of the stereoregular poly(*endo*-CHMA-*alt*-PO) (*cis* > 99%) in $CDCl_3$.

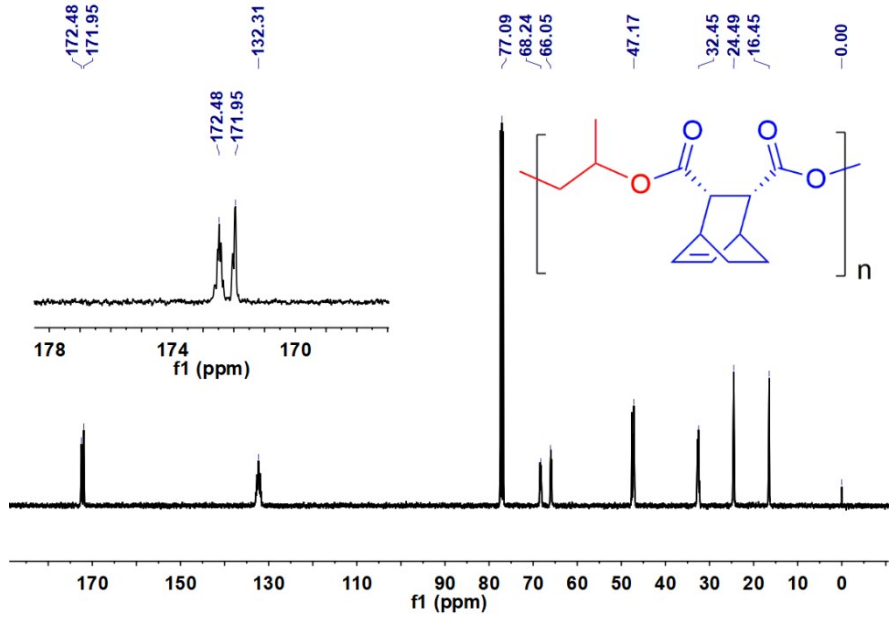

Figure S41. [13]C NMR spectrum of the stereoregular poly(*endo*-CHMA-*alt*-PO) (*cis* > 99%) in $CDCl_3$.

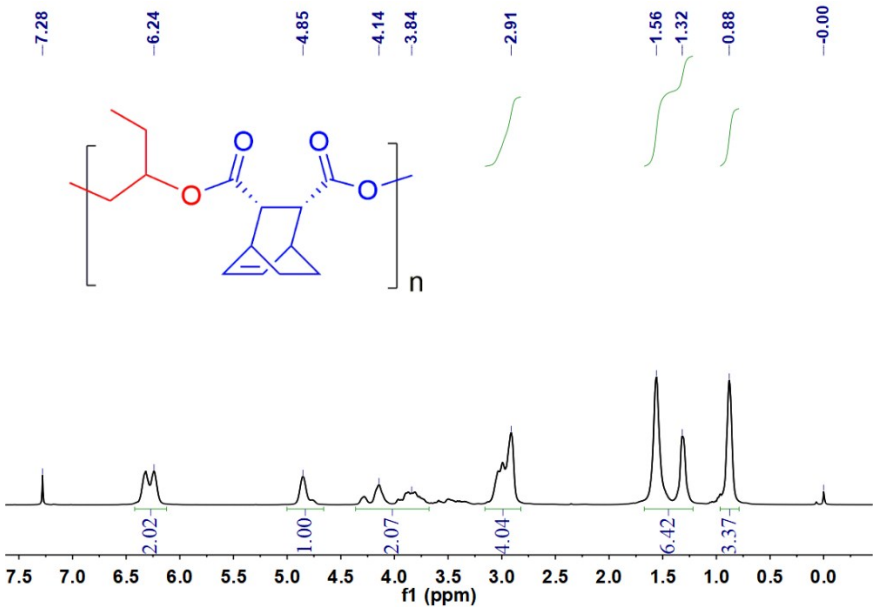

Figure S42. ^{1}H NMR spectrum of the stereoregular poly(*endo*-CHMA-*alt*-BO) (*cis* > 99%) in $CDCl_3$.

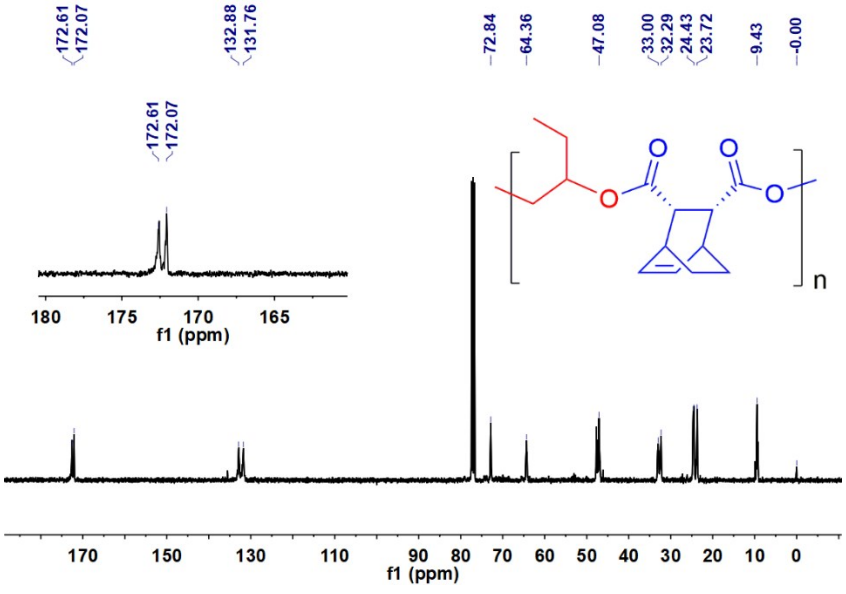

Figure S43. ^{13}C NMR spectrum of the stereoregular poly(*endo*-CHMA-*alt*-BO) (*cis* > 99%) in $CDCl_3$.

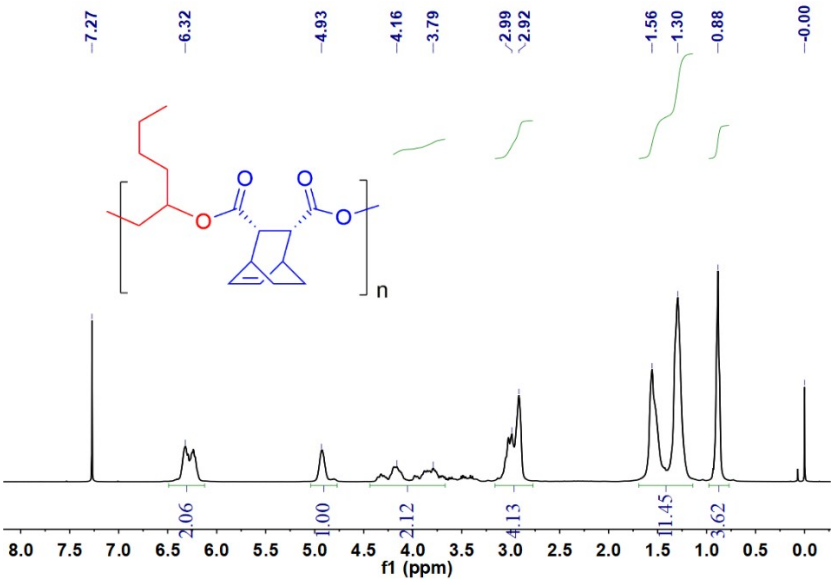

Figure S44. ^{1}H NMR spectrum of the stereoregular poly(*endo*-CHMA-*alt*-HO) (*cis* > 99%) in $CDCl_3$.

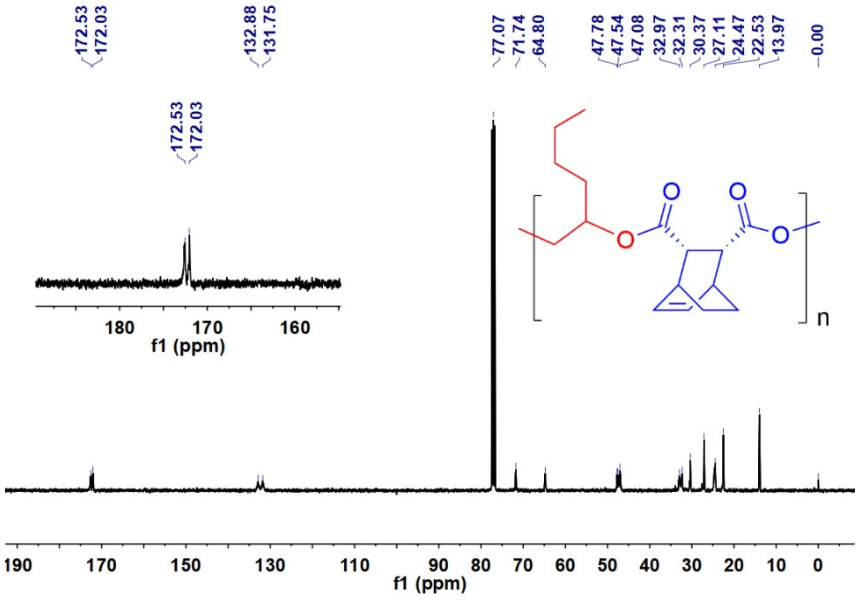

Figure S45. ^{13}C NMR spectrum of the stereoregular poly(*endo*-CHMA-*alt*-HO) (*cis* > 99%) in $CDCl_3$.

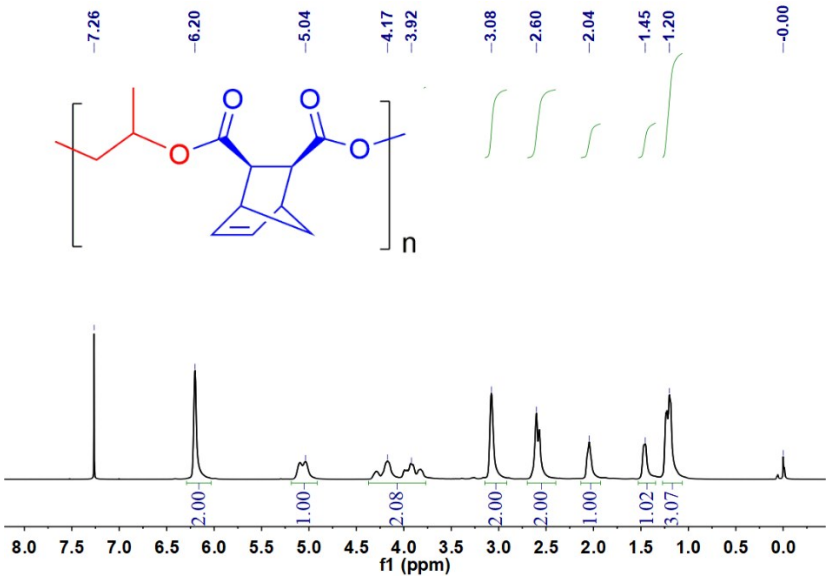

Figure S46. ^{1}H NMR spectrum of the stereoregular poly(*exo*-CPMA-*alt*-PO) (*cis* > 99%) in $CDCl_3$.

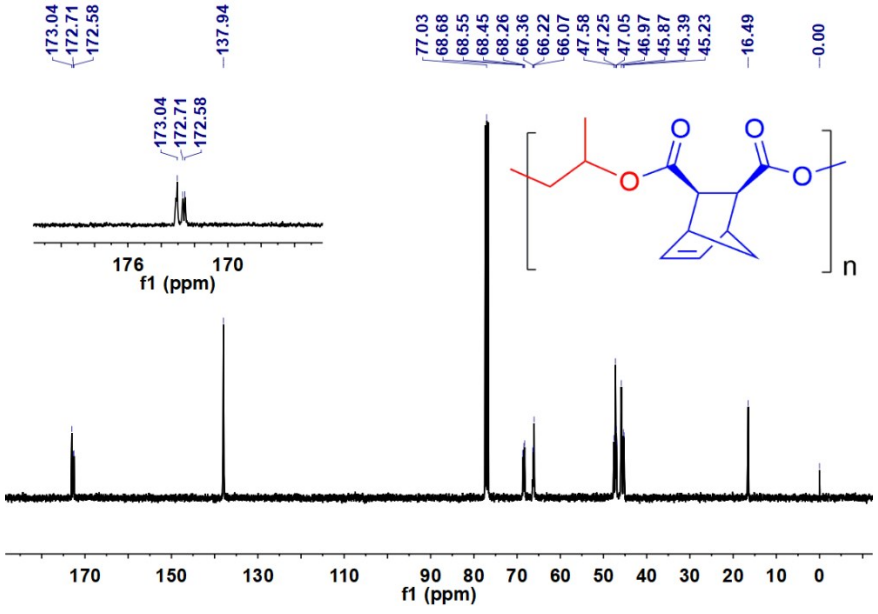

Figure S47. ^{13}C NMR spectrum of the stereoregular poly(*exo*-CPMA-*alt*-PO) (*cis* > 99%) in $CDCl_3$.

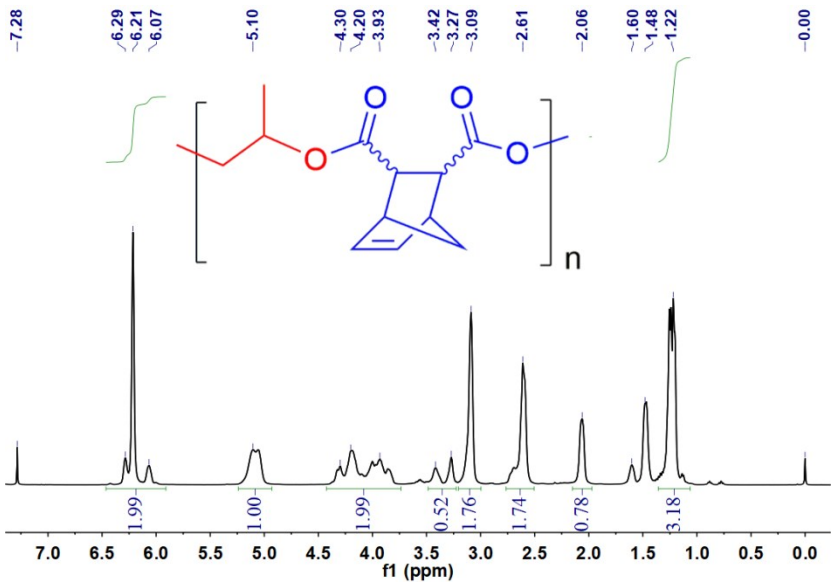

Figure S48. ^{1}H NMR spectrum of the stereoirregular poly(*exo*-CPMA-*alt*-PO) (*cis* = 87%) in $CDCl_3$.

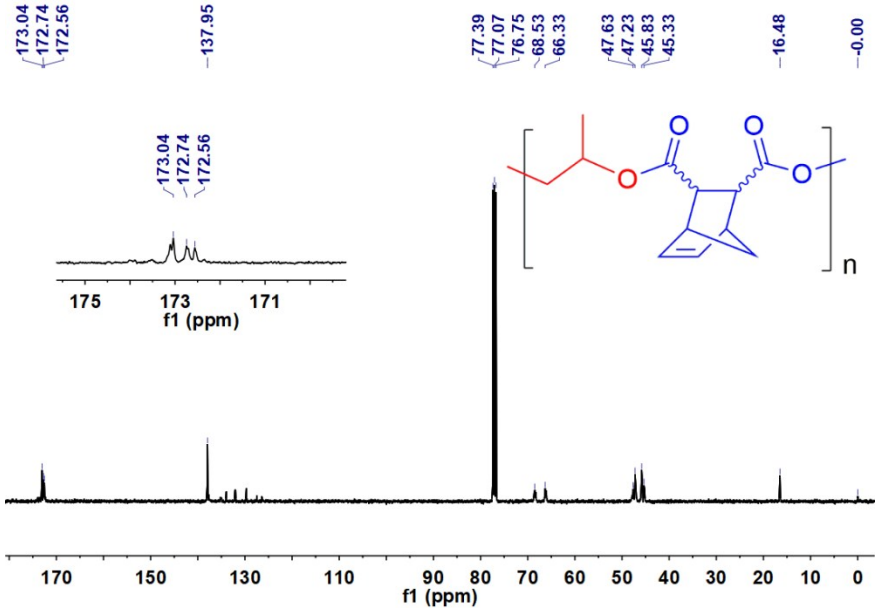

Figure S49. ^{13}C NMR spectrum of the stereoirregular poly(*exo*-CPMA-*alt*-PO) (*cis* = 87%) in $CDCl_3$.

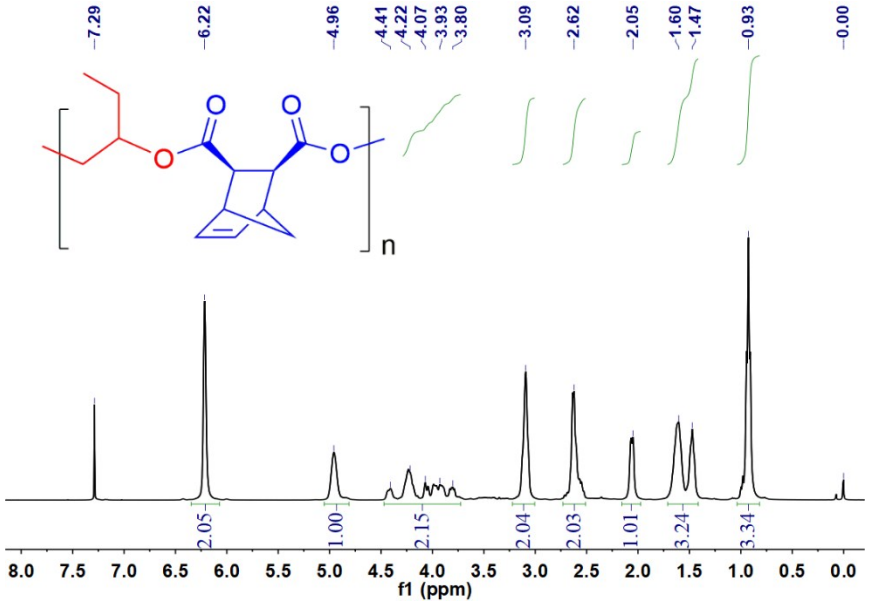

Figure S50. [1]H NMR spectrum of the stereoregular poly(*exo*-CPMA-*alt*-BO) (*cis* > 99%) in $CDCl_3$.

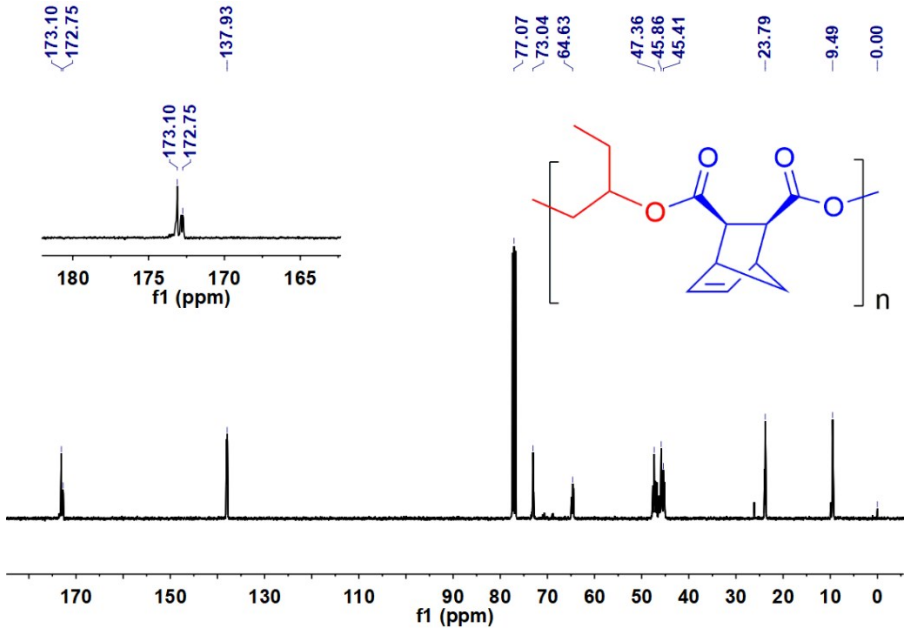

Figure S51. [13]C NMR spectrum of the stereoregular poly(*exo*-CPMA-*alt*-BO) (*cis* > 99%) in $CDCl_3$.

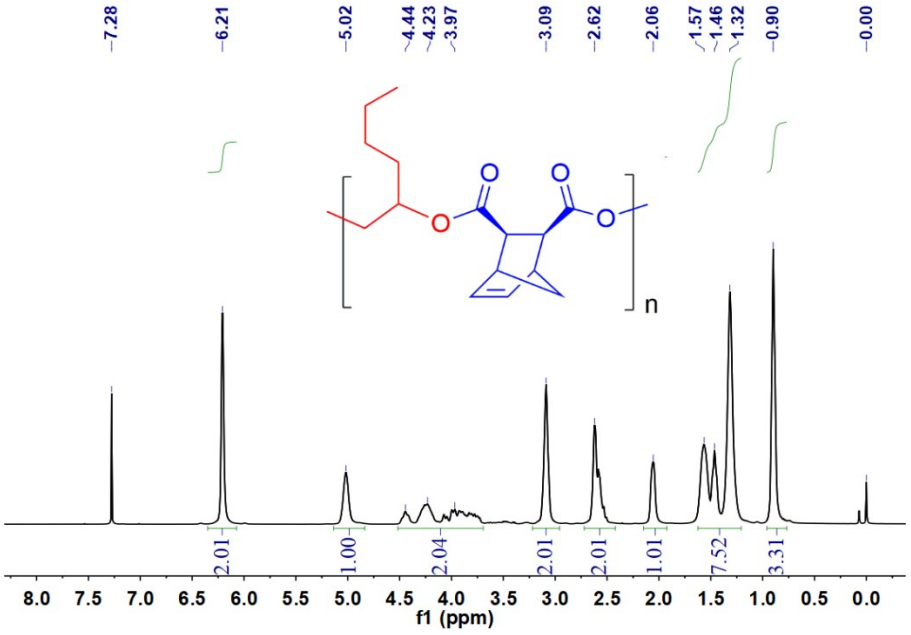

Figure S52. ^{1}H NMR spectrum of the stereoregular poly(*exo*-CPMA-*alt*-HO) (*cis* > 99%) in $CDCl_3$.

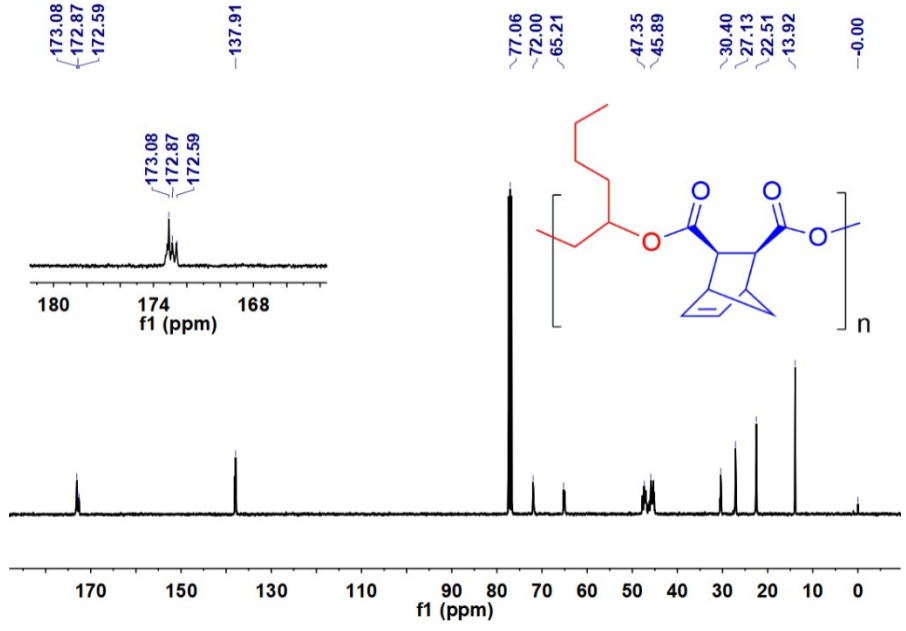

Figure S53. ^{13}C NMR spectrum of the stereoregular poly(*exo*-CPMA-*alt*-HO) (*cis* > 99%) in $CDCl_3$.

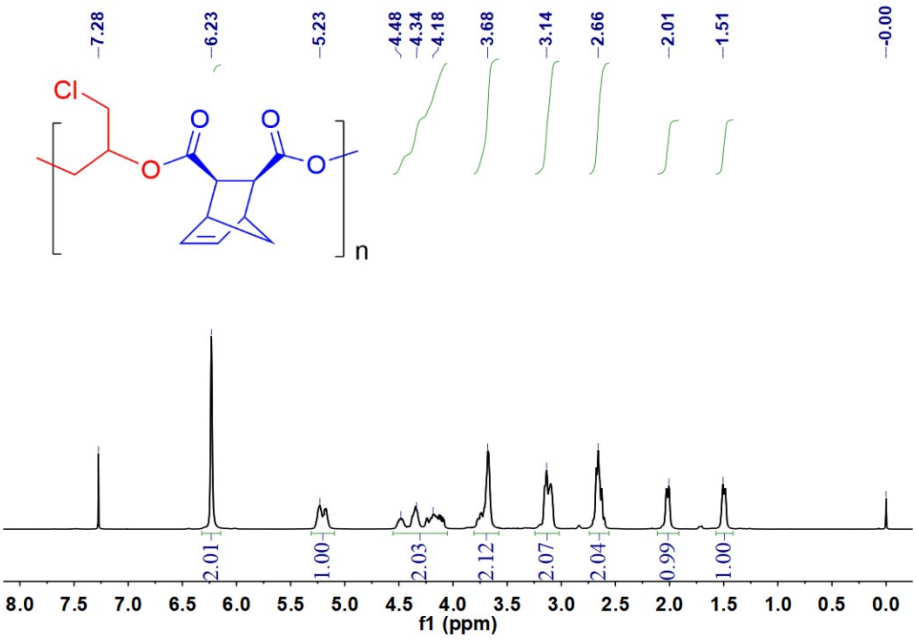

Figure S54. [1]H NMR spectrum of the stereoregular poly(*exo*-CPMA-*alt*-ECH) (*cis* > 99%) in $CDCl_3$.

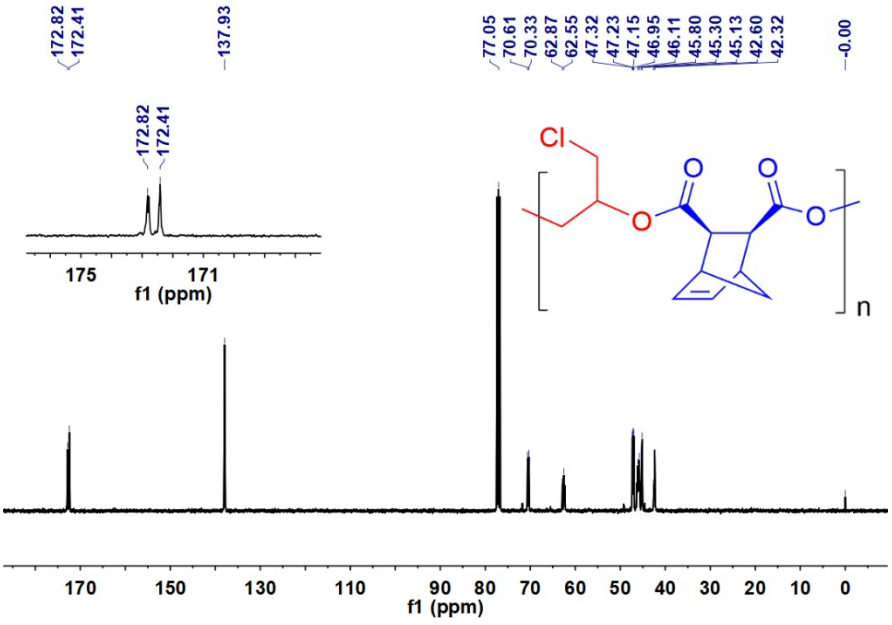

Figure S55. [13]C NMR spectrum of the stereoregular poly(*exo*-CPMA-*alt*-ECH) (*cis* > 99%) in $CDCl_3$.

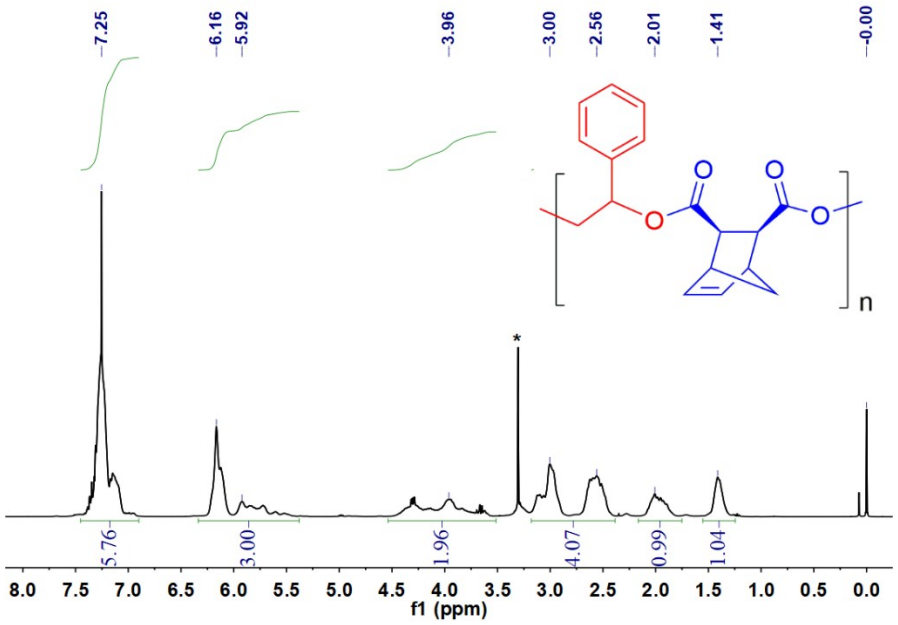

Figure S56. [1]H NMR spectrum of the stereoregular poly(*exo*-CPMA-*alt*-SO) (*cis* > 99%) in $CDCl_3$.

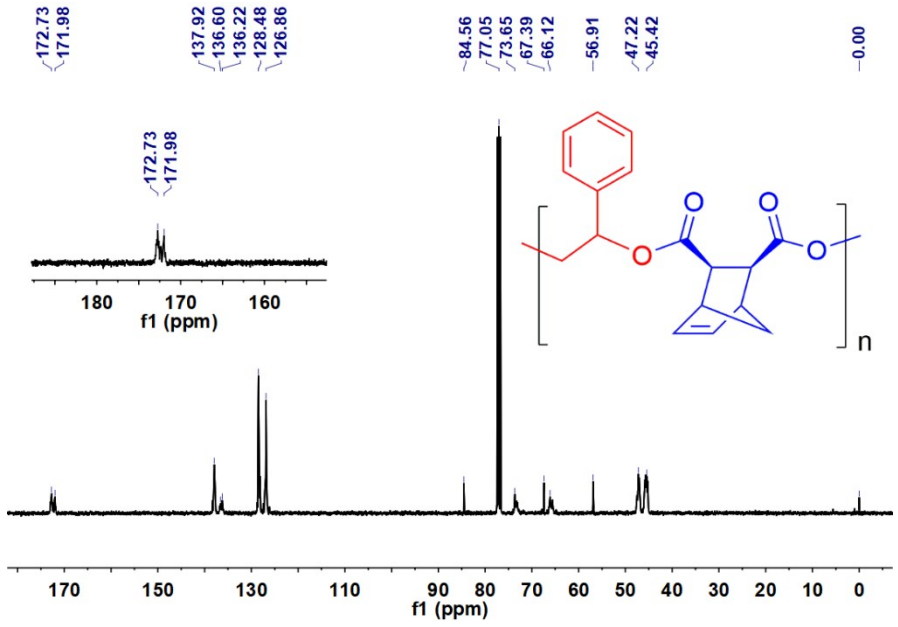

Figure S57. [13]C NMR spectrum of the stereoregular poly(*exo*-CPMA-*alt*-SO) (*cis* > 99%) in $CDCl_3$.

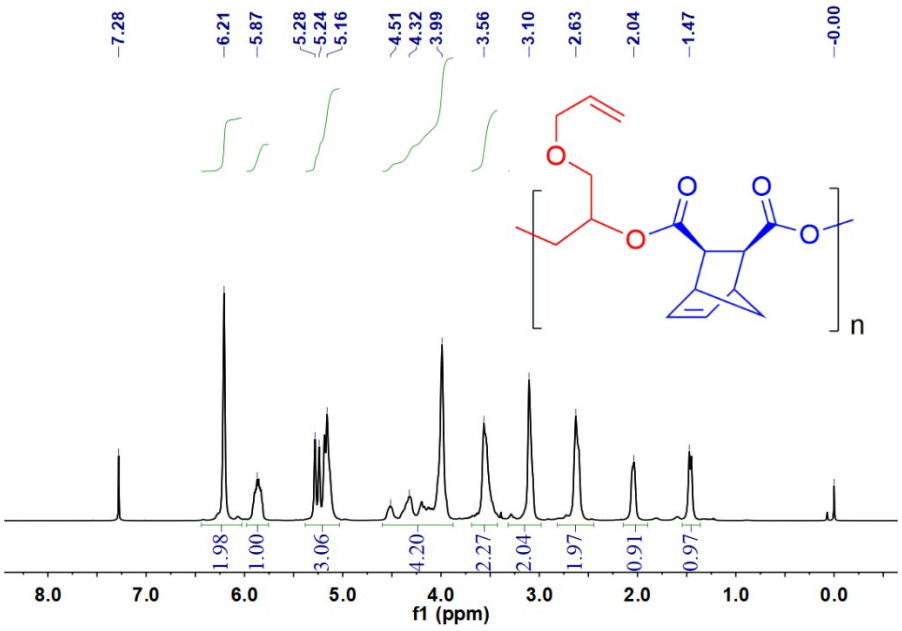

Figure S58. ^{1}H NMR spectrum of the stereoregular poly(*exo*-CPMA-*alt*-AGE) (*cis* > 99%) in $CDCl_3$.

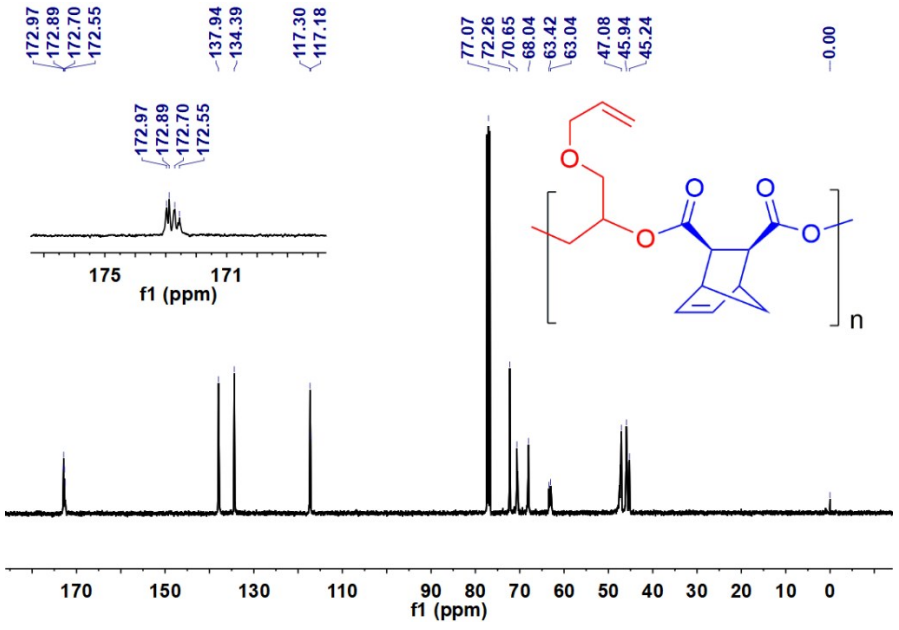

Figure S59. ^{13}C NMR spectrum of the stereoregular poly(*exo*-CPMA-*alt*-AGE) (*cis* > 99%) in $CDCl_3$.

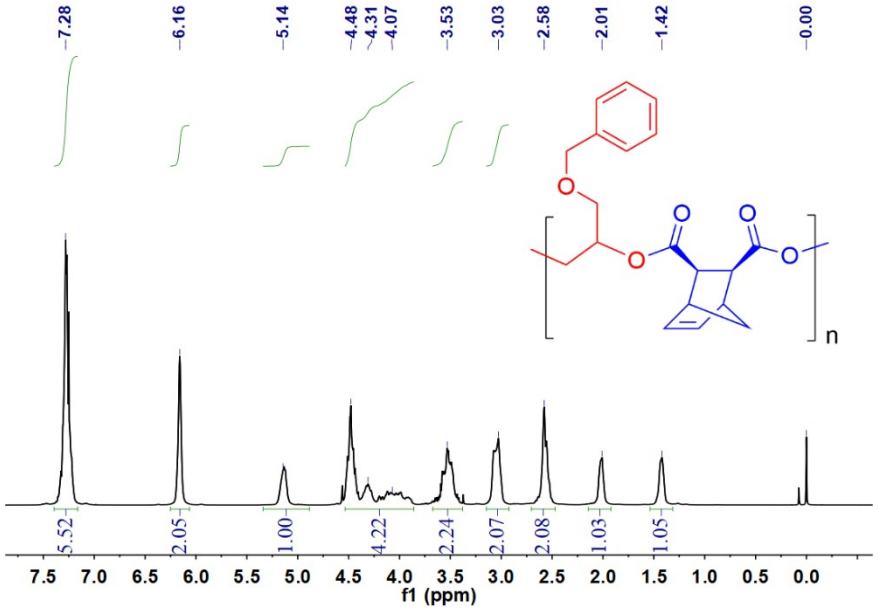

Figure S60. ^{1}H NMR spectrum of the stereoregular poly(*exo*-CPMA-*alt*-BGE) (*cis* > 99%) in $CDCl_3$.

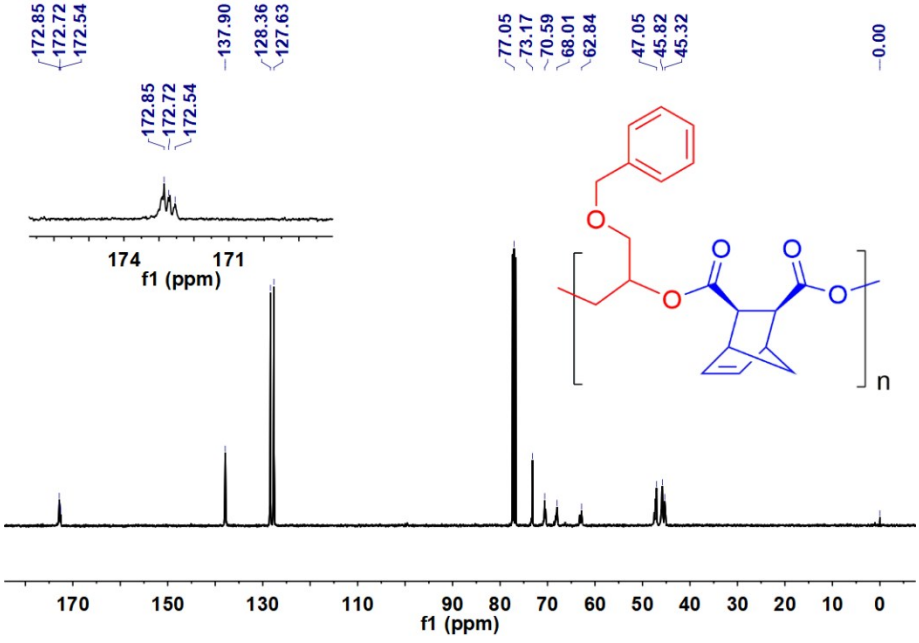

Figure S61. ^{13}C NMR spectrum of the stereoregular poly(*exo*-CPMA-*alt*-BGE) (*cis* > 99%) in $CDCl_3$.

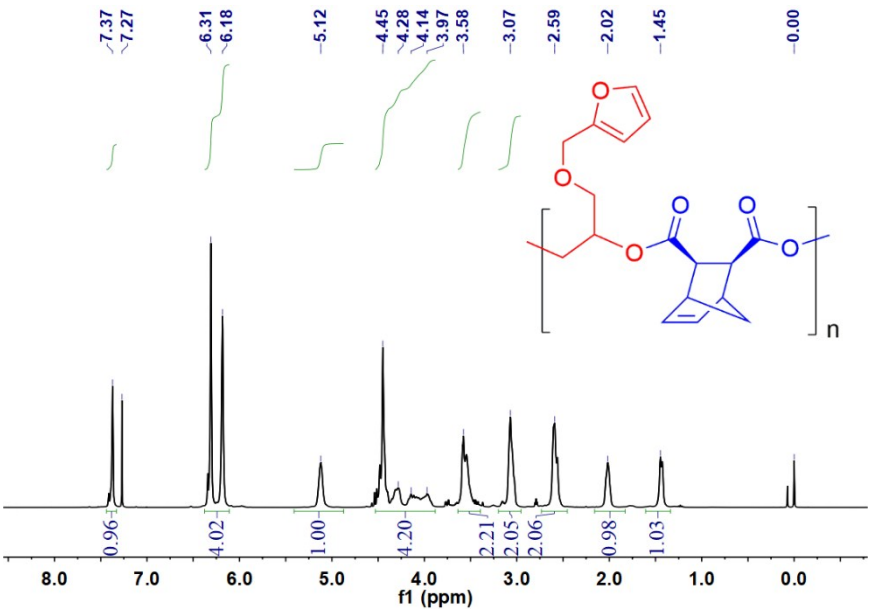

Figure S62. ^{1}H NMR spectrum of the stereoregular poly(*exo*-CPMA-*alt*-FGE) (*cis* > 99%) in $CDCl_3$.

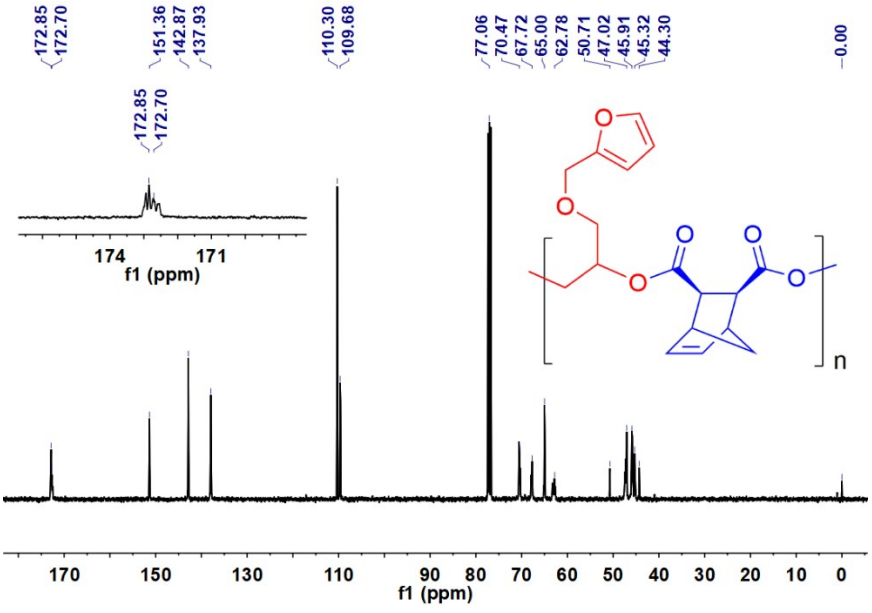

Figure S63. ^{13}C NMR spectrum of the stereoregular poly(*exo*-CPMA-*alt*-FGE) (*cis* > 99%) in $CDCl_3$.

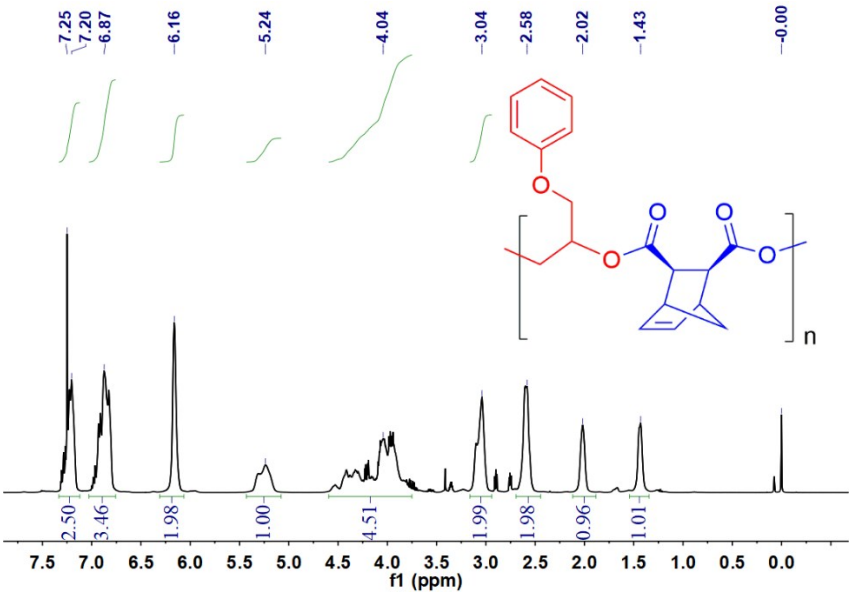

Figure S64. ^{1}H NMR spectrum of the stereoregular poly(*exo*-CPMA-*alt*-PGE) (*cis* > 99%) in $CDCl_3$.

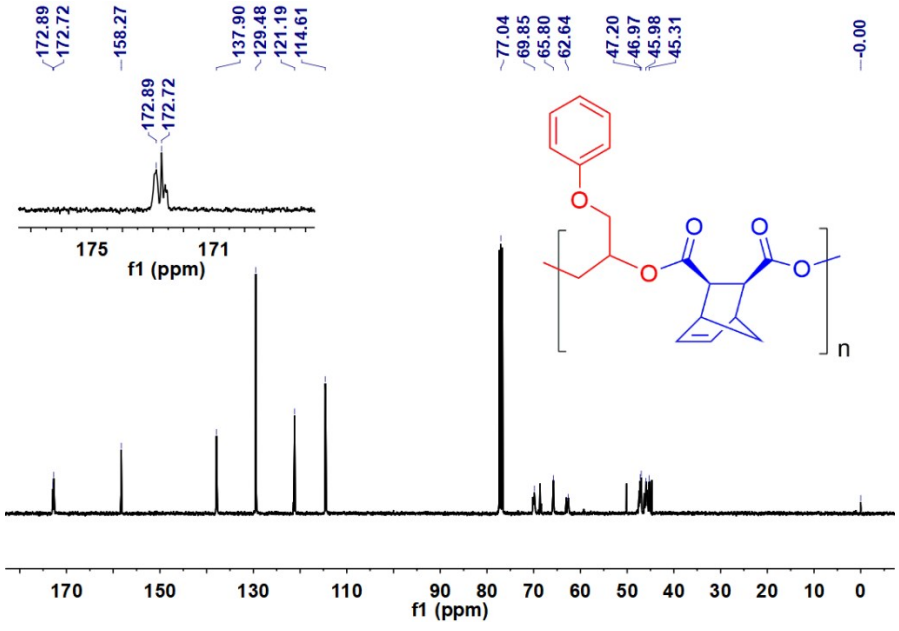

Figure S65. ^{13}C NMR spectrum of the stereoregular poly(*exo*-CPMA-*alt*-PGE) (*cis* > 99%) in $CDCl_3$.

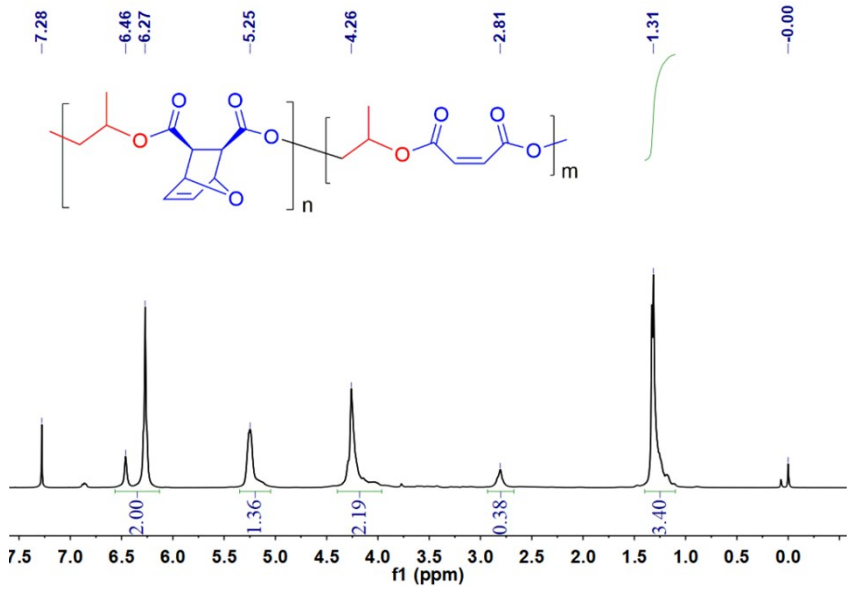

Figure S66. ^{1}H NMR spectrum of the stereoirregular poly(*exo*-FMA-*alt*-PO) (*cis* = 45%) in $CDCl_3$. Poly(propylene maleate) with a certain proportion (80%) was produced owing to retro Diels-Alder reaction of *exo*-FMA during the copolymerization process at 80 ºC. A decrease in reaction temperature to 40 ºC impressively reduced the percent of poly(propylene maleate) to 22%.

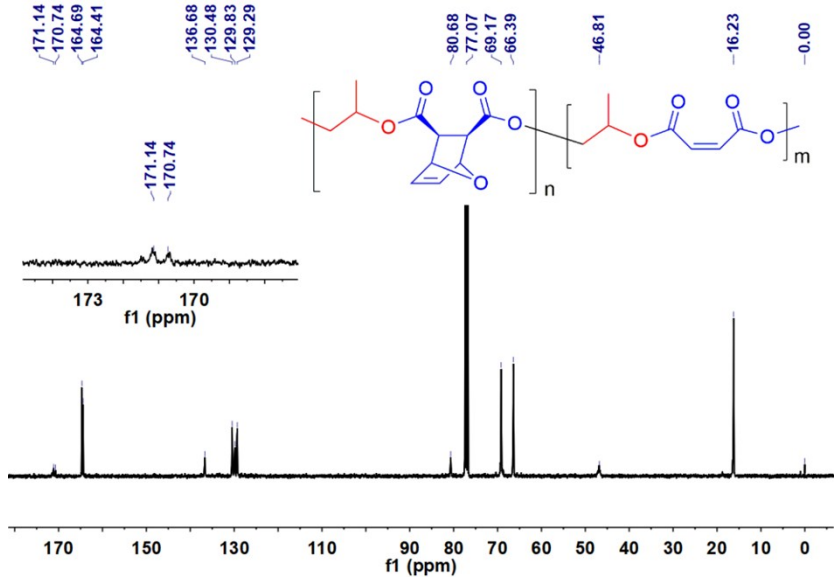

Figure S67. ^{13}C NMR spectrum of the stereoirregular poly(*exo*-FMA-*alt*-PO) (*cis* = 45%) in $CDCl_3$. Poly(propylene maleate) with a certain proportion (80%) was produced owing to retro Diels-Alder reaction of *exo*-FMA during the copolymerization process at 80 ºC. A decrease in reaction temperature to 40 ºC impressively reduced the percent of poly(propylene maleate) to 22%.

11. References

(1) H. Y. Ji, B. Wang, L. Pan and Y. S. Li, *Green Chem.*, 2018, **20**, 641-648.

(2) N. J. Van Zee, M. J. Sanford and G. W. Coates, *J. Am. Chem. Soc.*, 2016, **138**, 2755−2761.

(3) A. M. DiCiccio, J. M. Longo, G. G. Rodríguez-Calero and G. W. Coates, *J. Am. Chem. Soc.*, 2016, **138**, 7107−7113.

(4) J. Li, Y. Liu, W. M. Ren and X. B. Lu, *J. Am. Chem. Soc.*, 2016, **138**, 11493−11496.

(5) B. Han, L. Zhang, B. Liu, X. Dong, I. Kim, Z. Duan and P. Theato, *Macromolecules*, 2015, **48**, 3431−3437.

(6) A. Khan, S. Khan, I. Khan, C. Zhao, Y. Mao, Y. Chen and Y. J. Zhang, *J. Am. Chem. Soc.*, 2017, **139**, 10733−10741.